

Meiotic homologue alignment and its quality surveillance are controlled by mouse HORMAD1

Katrin Daniel¹, Julian Lange², Khaled Hached^{3,4}, Jun Fu⁵, Konstantinos Anastassiadis⁶, Ignasi Roig^{2,10}, Howard J. Cooke⁷, A. Francis Stewart⁵, Katja Wassmann^{3,4}, Maria Jasin⁸, Scott Keeney^{2,9} and Attila Tóth^{1,11}

Meiotic crossover formation between homologous chromosomes (homologues) entails DNA double-strand break (DSB) formation, homology search using DSB ends, and synaptonemal-complex formation coupled with DSB repair. Meiotic progression must be prevented until DSB repair and homologue alignment are completed, to avoid the formation of aneuploid gametes. Here we show that mouse HORMAD1 ensures that sufficient numbers of processed DSBs are available for successful homology search.

HORMAD1 is needed for normal synaptonemal-complex formation and for the efficient recruitment of ATR checkpoint kinase activity to unsynapsed chromatin. The latter phenomenon was proposed to be important in meiotic prophase checkpoints in both sexes. Consistent with this hypothesis, HORMAD1 is essential for the elimination of synaptonemal-complex-defective oocytes. Synaptonemal-complex formation results in HORMAD1 depletion from chromosome axes. Thus, we propose that the synaptonemal complex and HORMAD1 are key components of a negative feedback loop that coordinates meiotic progression with homologue alignment: HORMAD1 promotes homologue alignment and synaptonemal-complex formation, and synaptonemal complexes downregulate HORMAD1 function, thereby permitting progression past meiotic prophase checkpoints.

Physical linkages between homologues ensure correct chromosome segregation during the first meiotic division in mammals. These physical linkages, called chiasmata, depend on the formation of at least one reciprocal recombination event, or crossover, between each homologue pair and on cohesion between pairs of sister chromatids^{1,2} (Supplementary Fig. S1a). Crossover formation begins with the introduction of DSBs into the genome by the SPO11 enzyme^{3–5} (Supplementary Fig. S1). DSBs are processed to produce single-stranded DNA ends that can be used to probe for homology through strand invasion⁶. Several DSB ends work together on each homologue pair to ensure successful homologue alignment. After successful homology search, synaptonemal complexes form and connect the axes of aligned homologues. Synaptonemal-complex components promote post-homology search steps in DSB repair and are required for efficient crossover formation^{1,2}. After synaptonemal-complex formation, homology search is no longer needed and most DSBs are repaired through non-reciprocal recombination, which frequently results in gene conversion without the formation of

crossovers, while at least one DSB per chromosome pair is turned into a crossover^{1,2}. In mammals, meiotic checkpoint mechanisms eliminate meiocytes with defects in homologue alignment and DSB repair during the first meiotic prophase, thereby ensuring that gametes rarely form with an abnormal chromosome set or with unrepaired DNA (refs 7–14). Despite the importance of these meiotic prophase checkpoint mechanisms, they are poorly understood.

In various non-mammalian taxa, meiotic HORMA (Hop1, Rev7 and Mad2)-domain proteins have been implicated in diverse processes linked to crossover formation^{2,15–38}. These include DSB formation, homology search, preferred use of homologous DNA over sister DNA for repair of DSBs, synaptonemal-complex formation and the meiotic prophase checkpoint. Here we address the functions of HORMAD1, one of two meiosis-specific mouse HORMA-domain proteins (HORMAD1 and HORMAD2) that were shown to preferentially associate with unsynapsed chromosome axes during the first meiotic prophase in mice^{39–41}.

¹Institute of Physiological Chemistry, Technische Universität Dresden, Fiedlerstrasse 42, 01307 Dresden, Germany. ²Molecular Biology Program, Memorial Sloan-Kettering Cancer Center, New York, New York 10065, USA. ³CNRS UMR7622 Biologie du Développement, 9 quai St Bernard, Paris, 75005, France. ⁴UPMC Paris 6, 9 quai St Bernard, Paris, 75005, France. ⁵Genomics, BioInnovationsZentrum, Technische Universität Dresden, Am Tatzenberg 47, 01307 Dresden, Germany.

⁶Center for Regenerative Therapies Dresden, BioInnovationsZentrum, Technische Universität Dresden, Am Tatzenberg 47, 01307 Dresden, Germany. ⁷MRC Human Genetics Unit, Western General Hospital, Crewe Road, Edinburgh, EH4 2XU, UK. ⁸Developmental Biology Program, Memorial Sloan-Kettering Cancer Center, New York, New York 10065, USA. ⁹Howard Hughes Medical Institute, Memorial Sloan-Kettering Cancer Center, New York, New York 10065, USA. ¹⁰Present address: Unitat de Citologia i Histologia, Departamento Biología Celular, Fisiología i Immunología, Facultat de Biociències, Universitat Autònoma de Barcelona, Cerdanyola del Vallès, 08193, Spain.

¹¹Correspondence should be addressed to A.T. (e-mail: attila.Toth@mailbox.tu-dresden.de)

Received 15 October 2010; accepted 20 January 2011; published online 10 April 2011; DOI: 10.1038/ncb2213

RESULTS

HORMAD1 is required for fertility

Reasoning that functional analysis of HORMADs may provide new insights into meiotic chromosome behaviour and crossover formation in mammals, we disrupted *Hormad1* in mice (Supplementary Fig. S2). Whereas no obvious somatic defects were observed in *Hormad1*^{-/-} mice, both sexes are sterile, as reported previously⁴¹. Although spermatocytes in *Hormad1*^{-/-} mice are present in testis tubules at epithelial cycle stage III–IV, which we identified by the presence of intermediate spermatogonia⁴², they undergo apoptosis by the end of stage IV, and post-meiotic cells are not found in *Hormad1*^{-/-} testes (Supplementary Fig. S3). In the testes of wild-type mice, stage-IV tubules contain mid-pachytene spermatocytes⁴²; thus *Hormad1*^{-/-} spermatocytes are eliminated at a stage equivalent to mid-pachytene. As spermatocytes with defects in synaptonemal-complex formation and DSB repair are eliminated by the mid-pachytene checkpoint^{7–14}, we examined synaptonemal-complex formation on nuclear surface spreads of *Hormad1*^{-/-} spermatocytes.

HORMAD1 promotes synaptonemal-complex formation

In wild-type spermatocytes, chromosome axes are fully formed by late zygotene and synaptonemal-complex formation on autosomes is completed by pachytene (Fig. 1a,b). Whereas chromosome axis and cohesion core development and the timing of synaptonemal-complex formation are similar in wild-type and *Hormad1*^{-/-} spermatocytes, the efficiency of stable synaptonemal-complex initiation and synaptonemal-complex elongation is lower in the mutant (Fig. 1c and Supplementary Fig. S4). Autosomal synaptonemal-complex formation is never completed in *Hormad1*^{-/-} cells with fully formed chromosome axes ($n = 1,000$); most chromosomes that start synaptonemal-complex formation do not complete it, and many chromosomes do not even partially synapse (Fig. 1c). As a result of these defects, we cannot distinguish between late zygotene and pachytene in mutant spermatocytes and we refer to these stages as zygotene–pachytene. Unlike in meiocytes with a mutated synaptonemal-complex transverse filament, in which unsynapsed chromosomes align along their length^{8–11}, unsynapsed chromosomes do not align in *Hormad1*^{-/-} spermatocytes (Fig. 1c). Nevertheless, given the similar axis lengths of synapsed chromosomes, the relatively long stretches of synaptonemal complexes that frequently form in zygotene–pachytene *Hormad1*^{-/-} spermatocytes seem to connect homologues (Fig. 1c). Synaptonemal-complex formation between non-homologous chromosomes is unambiguously identifiable only in a small number of *Hormad1*^{-/-} spermatocytes (2.3% $n = 174$; data not shown). Similar homologue alignment and synaptonemal-complex formation defects are found in *Hormad1*^{-/-} oocytes (Supplementary Fig. S5). Others reported a complete lack of synaptonemal complexes in *Hormad1*^{-/-} spermatocytes, given the lack of tripartite synaptonemal-complex structures observable by electron microscopy⁴¹. The different conclusion reached by us may reflect differences in strain backgrounds and/or synaptonemal-complex-detection methods in the two studies.

Homologue-alignment defects may explain the synaptonemal-complex defects in the *Hormad1*^{-/-} mutant. Furthermore, HORMAD1 may also have synaptonemal-complex-promoting functions that are independent of its role in homologue alignment. To test this possibility, we examined the effect of the *Hormad1* mutation in the

DSB-deficient *Spo11*^{-/-} background, where homology search fails and synaptonemal complexes form extensively between non-homologous partners^{4,5} (Fig. 1). If HORMAD1 promotes synaptonemal-complex formation only through a function in DSB repair and homologue alignment, *Spo11*^{-/-} *Hormad1*^{-/-} double-mutant meiocytes should be as proficient in non-homologous synaptonemal-complex formation as *Spo11*^{-/-} single-mutant meiocytes. Notably, the double mutant has a much more severe synaptonemal-complex defect than either single mutant in both sexes (Fig. 1 and Supplementary Fig. S5). It is unlikely that the double-mutant synaptonemal-complex phenotype is caused by an early block in meiotic progression, because single- and double-mutant spermatocytes are eliminated at a comparable stage (Supplementary Fig. S6). Hence, our findings indicate that HORMAD1 promotes synaptonemal-complex formation independently of its role in homology search and raise the possibility that HORMAD1 has a direct role in synaptonemal-complex formation.

HORMAD1, DSB formation and DSB repair

Early DSB repair steps are important for homology search. Therefore, we examined whether defects in chromosome alignment and in synaptonemal-complex formation in *Hormad1*^{-/-} meiocytes reflect DSB-repair defects. The first step in DSB repair is DNA end resection, which creates single-stranded 3' overhangs bound by two recombinases, RAD51 and DMC1, that facilitate homology search^{1,2,6,43–45}. RAD51- and DMC1-marked meiotic DSB sites are chromosome-axes-associated, and RAD51–DMC1 focus counts provide an estimate of the number of DSBs available for homology search¹. Concomitant to synaptonemal-complex formation, RAD51 and DMC1 are replaced at most DSB sites by markers of intermediate stages of DSB repair, including the single-stranded DNA-binding proteins RPA (replication protein A) and MSH4 (MutS homologue 4; refs 1,46). Numbers of RAD51, DMC1, RPA and MSH4 foci are significantly lower in *Hormad1*^{-/-} spermatocytes than in wild-type cells during observable prophase stages⁴¹ (Fig. 2a–h and Supplementary Fig. S7a–d). During the comparable early–mid-zygotene stage, the median numbers of foci are threefold to sixfold lower in *Hormad1*^{-/-} spermatocytes (Fig. 2e–h). Numbers of RAD51 and RPA foci are also lower in *Hormad1*^{-/-} oocytes⁴¹ (Supplementary Fig. S7e,f). Thus, the steady-state numbers of single-stranded DSB ends seem much lower in *Hormad1*^{-/-} meiocytes, which may explain the inefficient homologue alignment and contribute to defective synaptonemal-complex formation.

Two scenarios may explain the lower numbers of processed DSB ends in *Hormad1*^{-/-} meiocytes: either fewer processed DSBs are produced, or DSBs are repaired faster. Recombination protein foci first appeared at similar times (but fewer in number) and did not disappear prematurely in *Hormad1*^{-/-} spermatocytes (Fig. 2e–h). In particular, we did not see a marked early reduction in the number of RPA foci, which would indicate premature repair. We also examined the behaviour of the late-recombination marker MutL homologue 1 (MLH1), which appears at destined crossover sites from mid-pachytene onwards in wild-type mice^{46–48} (Fig. 2i–k). We never observed MLH1 foci in *Hormad1*^{-/-} spermatocytes ($n = 378$). Formation of defective MLH1 foci in *Hormad1*^{-/-} spermatocytes⁴¹ is unlikely to be the result of a direct block in DSB repair, because MLH1 foci are detected (preferentially associated with synapsed axes) in *Hormad1*^{-/-}

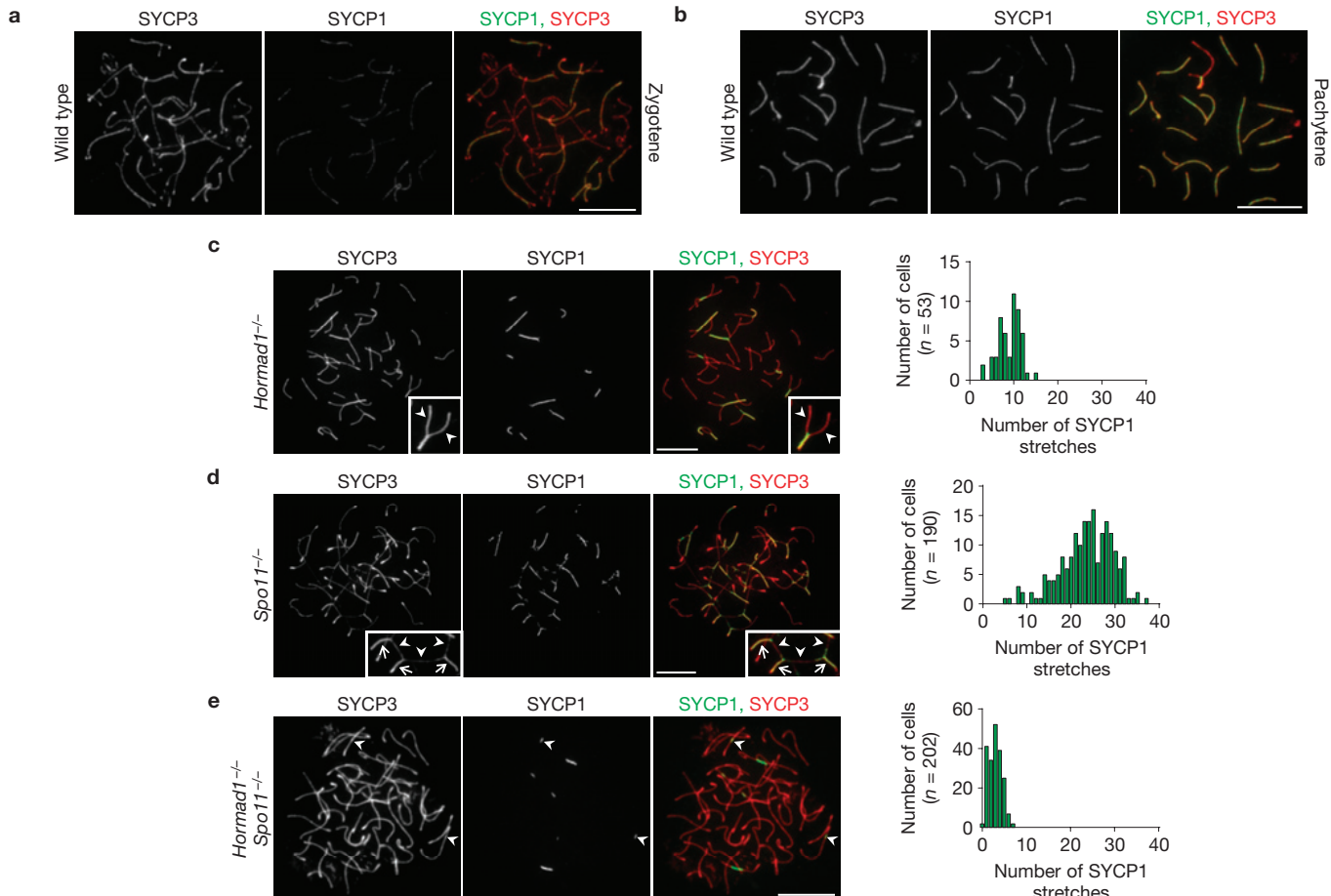


Figure 1 HORMAD1 promotes synaptonemal-complex formation independently of DSB-dependent processes. **(a–e)** Images of SYCP3 (chromosome axis) and SYCP1 (synaptonemal-complex transverse filament), detected by immunofluorescence microscopy on nuclear spreads of wild-type zygote (a), wild-type pachytene (b) and mutant zygote–pachytene (c–e left) spermatocytes collected from 14-week-old mice. **(c–e right)** The frequency distribution of synaptonemal-complex stretches in mutant zygote–pachytene spermatocytes. **(c)** Synaptonemal-complex formation is never completed on all autosomes in *Hormad1^{-/-}* cells, and unlike in meiocytes with a mutated synaptonemal-complex transverse filament, in which unsynapsed chromosomes align along their length^{8–11}, unsynapsed chromosomes do not align in *Hormad1^{-/-}* spermatocytes. Nevertheless, robust stretches of synaptonemal complex frequently form between

chromosomes that seem homologous on the basis of their similar axis lengths. Insets, enlarged view of a partially synapsed autosome: unsynapsed axes (arrowheads) are of similar lengths. **(d)** In contrast, synaptonemal complexes connect multiple non-homologous axes, thereby creating a meshwork of interconnected axes in the *Spo11^{-/-}* mutant, in which strand invasion and homology search are not possible owing to the lack of DSBs. Insets, enlarged view of chromosome axes: arrowheads mark unsynapsed, arrows mark synapsed axes. **(e)** Both the number and the length of SYCP1 stretches are lower in *Hormad1^{-/-} Spo11^{-/-}* spermatocytes, relative to the single mutants. Most (61% in n=144 cells) of the remaining SYCP1 stretches are unambiguously linked to a single chromosome axis (arrowheads), indicating that SYCP1 stretches do not necessarily mark inter-chromosomal synaptonemal complexes. Scale bars, 10 µm.

oocytes, albeit in lower numbers (~30% of MLH1 foci numbers in wild-type oocytes; Fig. 2i–k). This difference between oocytes and spermatocytes is probably due to the different timings of elimination of defective meiocytes, with oocytes eliminated later, allowing stages corresponding to late pachytene to be examined. Although we cannot exclude that some DSB repair steps are accelerated in *Hormad1^{-/-}* meiocytes, the behaviour of recombination proteins does not indicate significant acceleration.

We next investigated how efficiently DSBs and/or single-stranded DSB ends are produced in the *Hormad1^{-/-}* mutant. DSBs trigger accumulation of phospho-histone H2AX (γH2AX) during leptotene/early-zygotene through activation of ATM kinase^{49,50}. Levels of chromatin-bound γH2AX are significantly lower in *Hormad1^{-/-}* leptotene/early-zygotene spermatocytes (Supplementary Fig. S8). Consistent with this, others reported lower γH2AX levels and lower levels

of ATM autophosphorylation, implying lower levels of ATM activation, in *Hormad1^{-/-}* spermatocytes⁴¹.

As this result may indicate lower levels of DSB formation, we measured the effect of *Hormad1^{-/-}* mutation on the amounts of SPO11–oligonucleotide complexes that are produced when DSB ends are resected⁴⁵ (Fig. 3a–d). To control for the fact that the *Hormad1^{-/-}* mutant exhibits a mid-pachytene spermatogenic block, we employed the DSB-repair-defective *Dmc1^{-/-}* background: DMC1-deficient spermatocytes arrest in mid-pachytene irrespective of *Hormad1* genotype^{12,43,44} (Fig. 3e). In three independent experiments with adult mice, we observed a 2-, 3.1- and 4.2-fold reduction in testis-weight-normalized SPO11–oligonucleotide levels in *Hormad1^{-/-} Dmc1^{-/-}* testes, relative to *Hormad1^{+/+} Dmc1^{-/-}* controls (Fig. 3a). We also examined SPO11–oligonucleotide levels in testes of juvenile, 14 days postpartum (dpp), mice (Fig. 3c), in which the sizes and cellularities

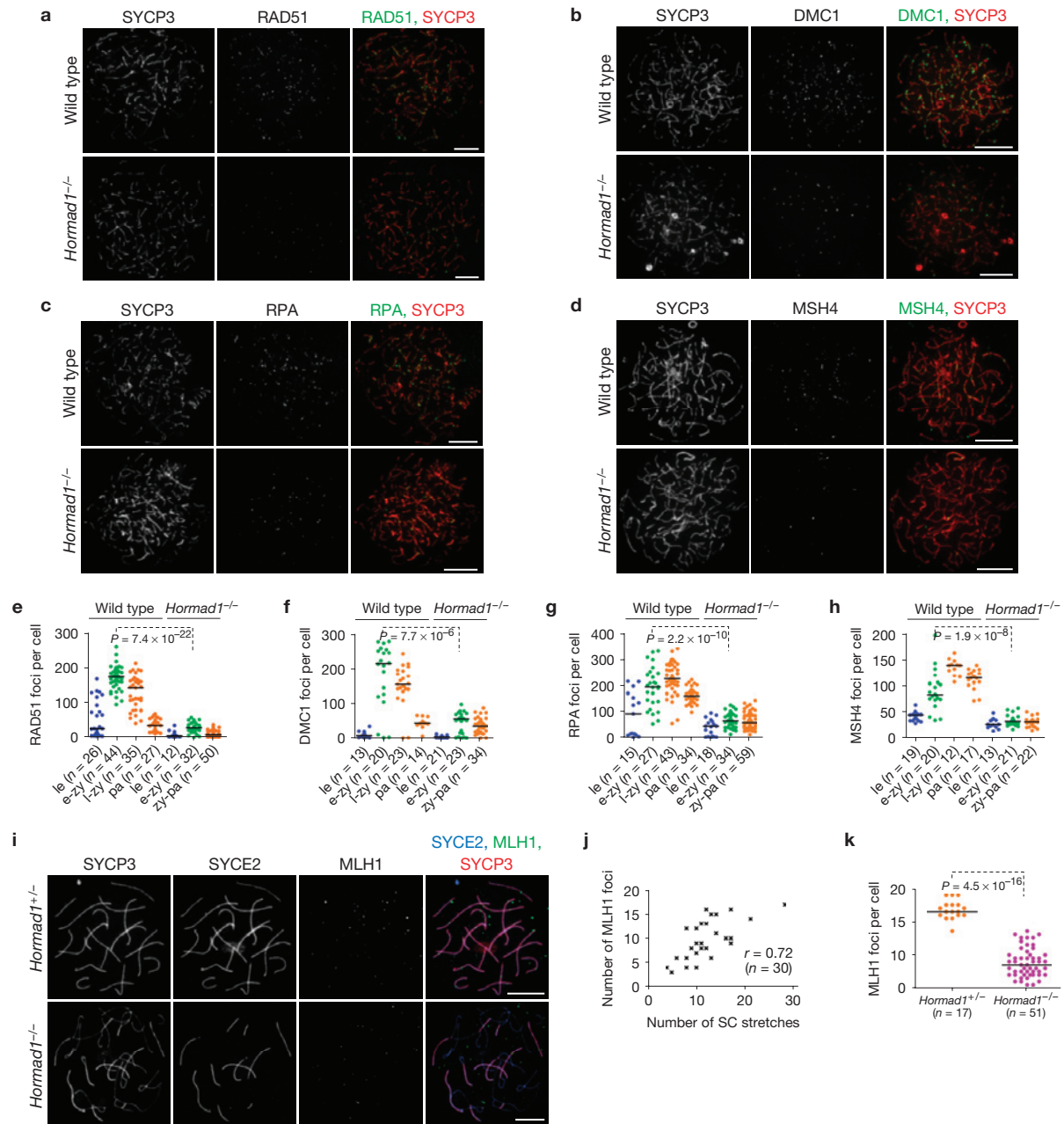


Figure 2 Numbers of early-, intermediate- and late-recombination-protein foci are lower in the absence of HORMAD1 in prophase meiocytes. (a–d) SYCP3 and either RAD51 (a), DMC1 (b), RPA (c) or MSH4 (d) are detected on nuclear spreads of typical early-mid-zygote wild-type and Hormad1^{-/-} spermatocytes from 16-day-old mice. Scale bars, 10 μ m. (e–h) Numbers of early (RAD51, e; DMC1, f) and intermediate (RPA, g; MSH4, h) recombination protein foci during leptotene (le) and early-mid-zygote (e-zy) in wild-type and Hormad1^{-/-}, late zygote (l-zy) and pachytene (pa) in wild-type and zygote-pachytene (zy-pa) in Hormad1^{-/-} spermatocytes. Median numbers of foci are marked. During the comparable early-mid-zygote stage, a threefold to sixfold reduction (highly significant by Mann–Whitney test) is observed in the numbers of recombination protein foci in the mutant relative to wild-type spermatocytes. (i–k) The numbers of crossover marker MLH1 foci are lower in the absence of HORMAD1 in oocytes. (i) SYCP3 (chromosome axis), SYCE2 (synaptonemal-complex central element) and MLH1 were detected

by immunofluorescence microscopy in nuclear spreads of Hormad1^{+/-} and Hormad1^{-/-} oocytes from 19.5 dpc fetuses (a stage when most oocytes are in the late pachytene or diplotene stage in wild-type mice). Fewer chromosome-axis-associated MLH1 foci are detected in Hormad1^{-/-} oocytes than in Hormad1^{+/-} oocytes. Note that most MLH1 foci (78%, $n = 51$ cells) are observed on synapsed axes in the mutant. Scale bars, 10 μ m. (j) Scatter plot shows positive correlation (Spearman's $r = 0.72, n = 30$) between the number of MLH1 foci and the number of synaptonemal-complex (SC) stretches (immunostaining for SYCE1 or SYCE2) in Hormad1^{-/-} oocytes, indicating that DSBs may be repaired as crossovers preferentially in chromosome regions that align and synapse, or that synapsis occurs preferentially where crossovers are successfully designated. (k) The number of chromosome-axis-associated MLH1 foci is approximately threefold lower in Hormad1^{-/-} oocytes from 18.5 to 19.5 dpc fetuses, relative to Hormad1^{+/-} oocytes. Median numbers of foci are marked by horizontal lines.

of wild-type and mutant testes are comparable because most spermatocytes have not yet progressed far enough in meiosis to be affected by

the mid-pachytene checkpoint. In two independent experiments, testis-weight-normalized SPO11–oligonucleotide levels were 3.8- and 4.8-

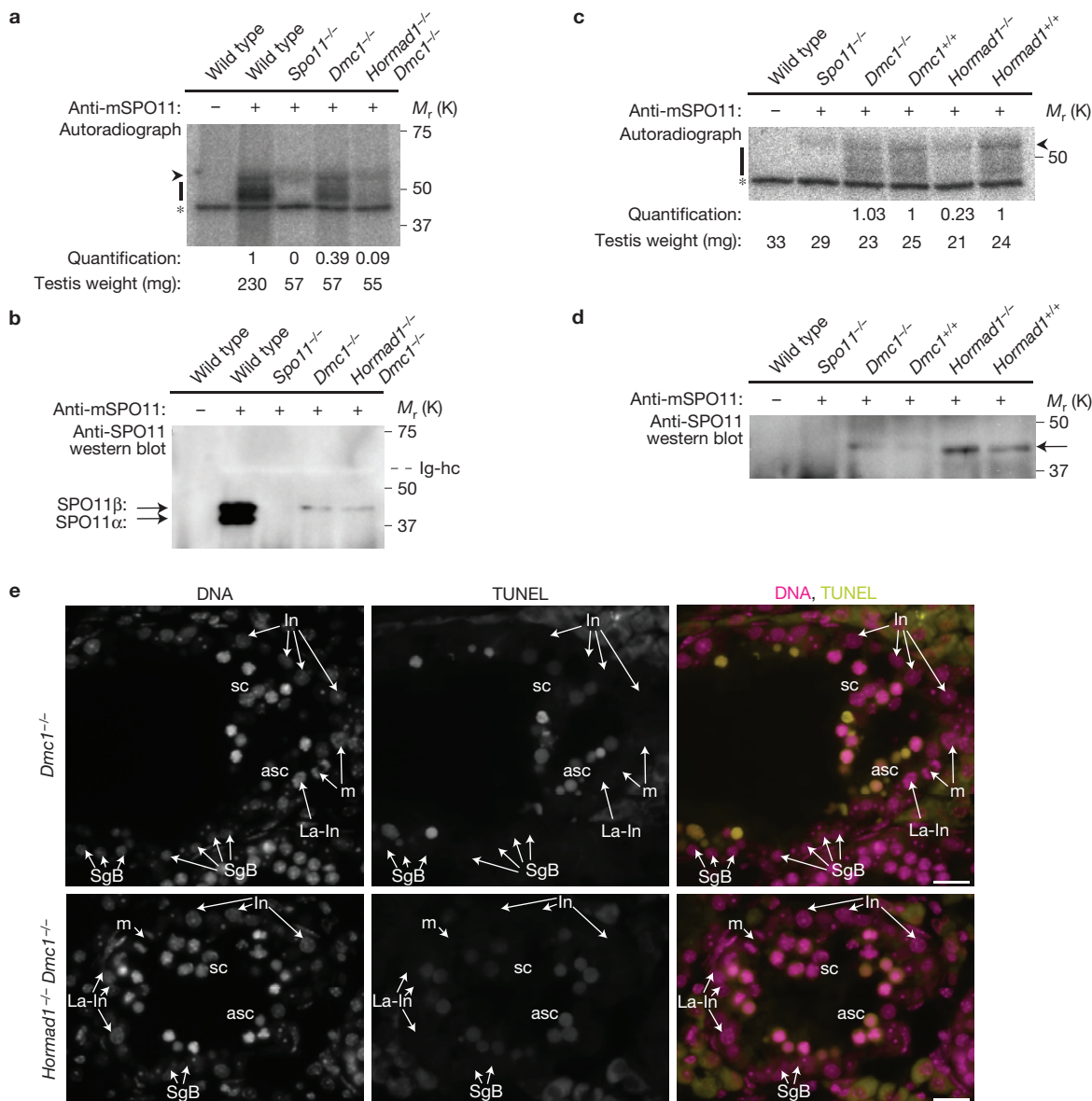


Figure 3 Amounts of SPO11–oligonucleotide complexes in testes are lower in the absence of HORMAD1. **(a–d)** Levels of SPO11–oligonucleotide complexes and SPO11 protein were examined in the testes of the indicated mouse strains. **(a,c)** Measurement of SPO11–oligonucleotide complexes in testes of adult 14-week-old **(a)** and juvenile 14-dpp **(c)** mice. SPO11–oligonucleotide complexes were immunoprecipitated with or without anti-SPO11 antibodies, and covalently linked oligonucleotides were radioactively labelled. Each sample represents one-testis-equivalent SPO11–oligonucleotide complexes. Bars mark SPO11-specific signals and asterisks indicate nonspecific labelling of a contaminant in the terminal deoxytransferase preparations. Ig-hc marks an artefactual radioactive signal attributable to the presence of immunoglobulin heavy chain (Ig-hc in **b**). Quantified radioactive signals in the mutants have been background-corrected and normalized: in **a** signals are normalized to the adult wild-type control; in **c** *Dmc1^{-/-}* and *Hormad1^{-/-}* signals are normalized to their littermate *Dmc1^{+/-}* and *Hormad1^{+/-}* controls, respectively (see Methods). Blots of immunoprecipitates from **a** and **c** were probed with anti-SPO11 antibodies in **b** and **d**, respectively. **(b)** In wild-type adults, two alternative forms of SPO11 (α and β) are present⁵. Total SPO11

amounts are similar in *Dmc1^{-/-}* and *Hormad1^{-/-} Dmc1^{-/-}* mutants, and are lower in the mutants than in wild-type controls. Only SPO11 β , the form that appears early in meiosis, is detected in the mutants. Arrowhead marks the immunoglobulin heavy chain (bleached out signal). Mid-pachytene spermatogenetic block in the mutants (**e**) is the likely cause of the lower SPO11 amounts in *Dmc1^{-/-}* and *Hormad1^{-/-} Dmc1^{-/-}* testes, and of the lower SPO11–oligonucleotide amounts in *Dmc1^{-/-}* testes^{12,43,44}. **(d)** In juveniles, total SPO11 protein levels are low and only the long β form of SPO11 (arrow) is detectable⁵. For full-scan gel images of **a–d**, see Supplementary Fig. S10. **(e)** DNA was detected by DAPI, and apoptosis was detected by an IF-TUNEL assay on cryosections of testes of 15-week-old mice. *Dmc1^{-/-}* and *Hormad1^{-/-} Dmc1^{-/-}* spermatocytes undergo apoptosis in stage-IV tubules, as identified by the concomitant presence of intermediate spermatogonia (In), late-prometaphase intermediate spermatogonia (La-In), mitotic intermediate spermatogonia (m) and spermatogonia B (SgB). Both non-apoptotic (sc) and apoptotic (asc) spermatocytes are present in the stage-IV tubules shown. Spermatocytes are fully eliminated on progression to stage V (data not shown). Scale bars, 20 μ m.

fold lower in *Hormad1^{-/-}* testes, relative to wild-type controls, whereas those for wild-type and *Dmc1^{-/-}* testes were similar. Although we cannot exclude that turnover of both SPO11–oligonucleotide complexes

and single-stranded DSB ends are faster in the *Hormad1^{-/-}* mutant, the simplest interpretation of our observations is that HORMAD1 is needed for efficient formation of DSBs and/or single-stranded DSB ends.

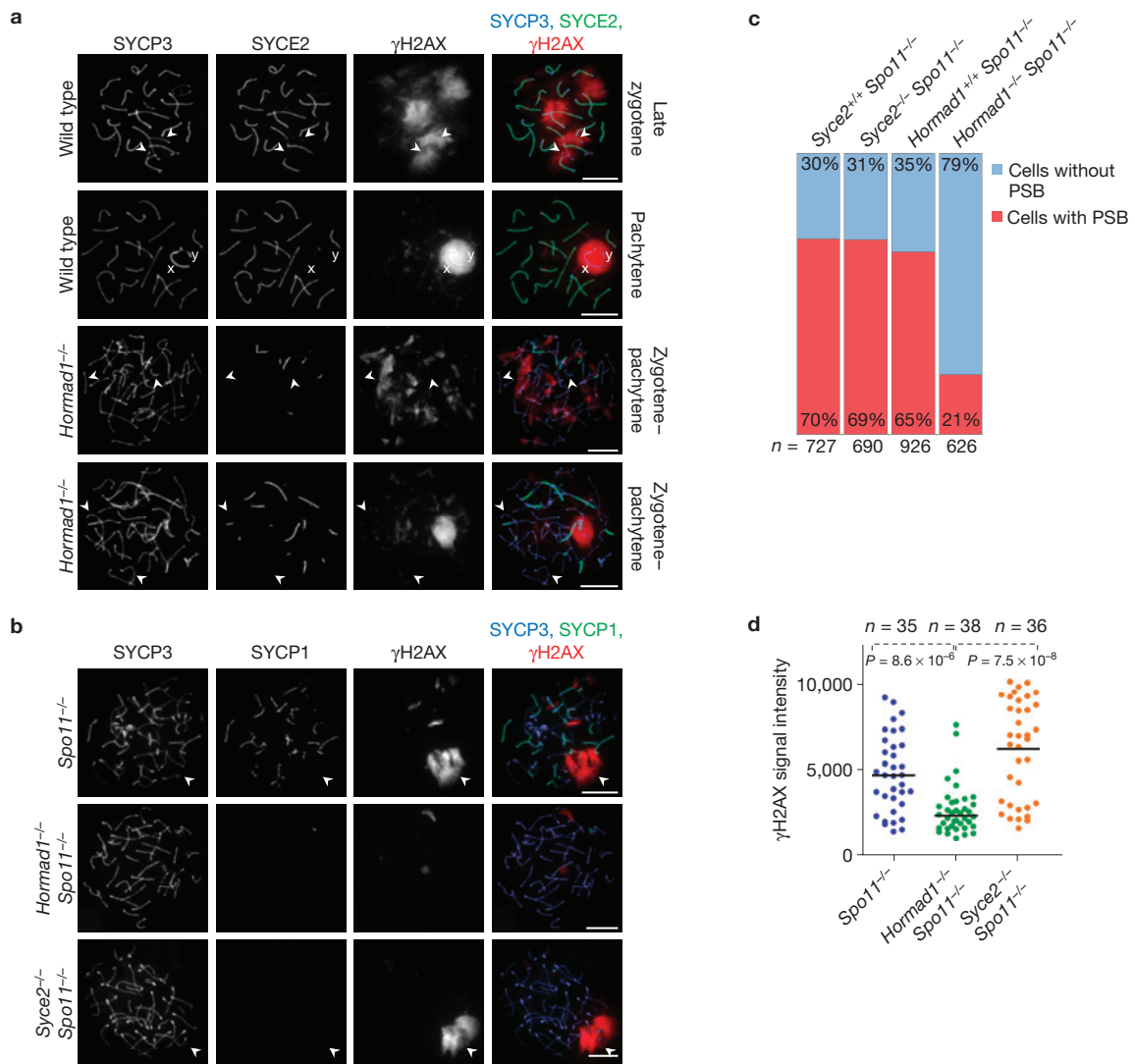


Figure 4 HORMAD1 is required for sex-body and pseudo-sex-body formation in the *Spo11*^{+/+} and *Spo11*^{-/-} backgrounds, respectively. **(a)** SYCP3 (chromosome axis), SYCE2 (synaptonemal-complex central element) and γH2AX were detected in nuclear spreads of wild-type late-zygotene and pachytene, and *Hormad1*^{-/-} zygote–pachytene spermatocytes collected from 16-day-old mice. Matched-exposure images of γH2AX are shown. In wild-type late-zygotene spermatocytes, γH2AX chromatin domains associate with unsynapsed chromosome axes. In wild-type pachytene cells, unsynapsed regions of X and Y sex-chromosome axes (marked by x and y) are surrounded by one large γH2AX-rich chromatin domain, the sex body. Anti-γH2AX staining is patchy in most (59%) *Hormad1*^{-/-} spermatocytes, with no clear correlation between lack of synapsis and γH2AX localization (third row). A few large γH2AX-rich chromatin domains form in a small number of *Hormad1*^{-/-} spermatocytes (41%, n = 512), but only a subset of unsynapsed axes overlap with γH2AX-rich chromatin, and synapsed axes overlapping with γH2AX-rich chromatin domains are also observed

regularly (bottom row). Arrowheads mark two unsynapsed axes in wild-type late-zygotene spermatocytes and in each mutant cell type. Scale bars, 10 μm. **(b)** Matched-exposure images of SYCP3 (chromosome axis), SYCP1 (synaptonemal-complex transverse filament) and γH2AX in nuclear spreads of *Spo11*^{-/-}, *Hormad1*^{-/-} *Spo11*^{-/-} and *Syce2*^{-/-} *Spo11*^{-/-} spermatocytes of adult (9-week-old) mice. Large γH2AX-rich chromatin domains (pseudo-sex bodies marked by arrowheads) frequently form in *Spo11*^{-/-} and *Syce2*^{-/-} *Spo11*^{-/-} spermatocytes. Scale bars, 10 μm. **(c)** Quantification of pseudo-sex-body formation in spermatocytes with full-length chromosome axes (collected from 24-day-old mice). The percentage of cells with no pseudo-sex body (cells without PSB) or with one to three clear pseudo-sex bodies (cells with PSB) is shown. **(d)** Quantification of the γH2AX signal in spermatocytes with full-length chromosome axes (collected from 24-day-old mice). There is a significant reduction in total nuclear γH2AX amounts in spermatocytes from *Hormad1*^{-/-} *Spo11*^{-/-} mice, relative to spermatocytes from *Spo11*^{-/-} and *Syce2*^{-/-} *Spo11*^{-/-} mice (Mann–Whitney test).

HORMAD1 and meiotic prophase checkpoints

Collaboration between Hop1 and Mec1, the yeast orthologues of HORMAD1 and ATR respectively, is required for the meiotic prophase checkpoint in budding yeast³⁵. Interestingly, HORMAD1 preferentially associates with unsynapsed chromosome axes, resembling the behaviour of ATR and two ATR activators, BRCA1 and TOPBP1, in wild-type meiocytes^{51–57}. Active ATR phosphorylates H2AX on unsyn-

napsed chromatin from zygote onwards, thereby promoting meiotic silencing of unsynapsed chromosomes (MSUC), a phenomenon that is crucial for the mid-pachytene checkpoint^{13,14,57}. Therefore, we investigated whether HORMAD1 also has a role in these processes. In spermatocytes, sex chromosomes synapse and recombine only in their short pseudoautosomal regions. Consequently, most sex-chromosome regions remain unsynapsed and silenced in a γH2AX-rich structure

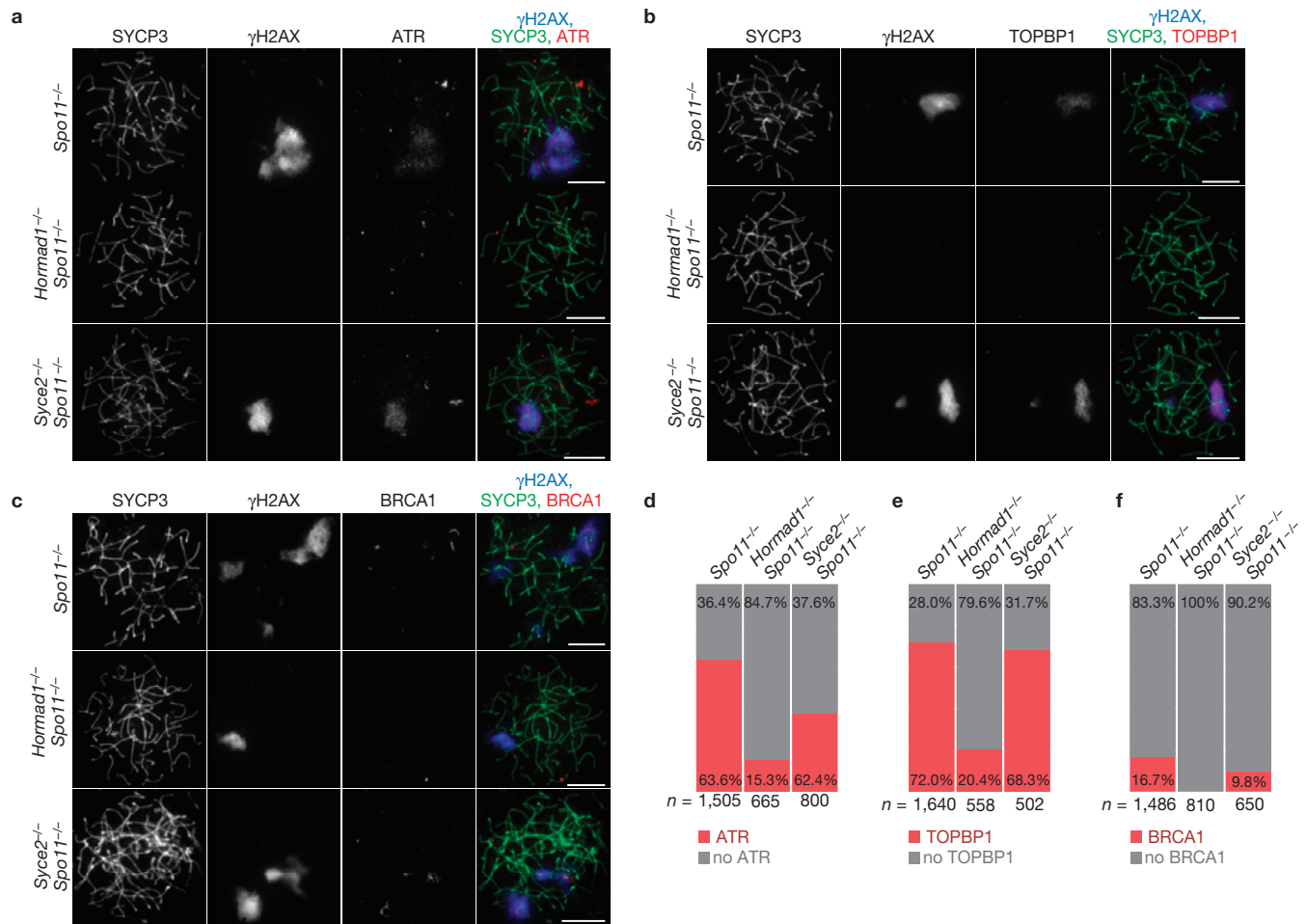


Figure 5 HORMAD1 is required for efficient accumulation of ATR, TOPBP1 and BRCA1 on chromatin in the absence of programmed DSBs. **(a–c)** Matched-exposure images of SYCP3 (chromosome axis), γ H2AX and either ATR **(a)**, TOPBP1 **(b)** or BRCA1 **(c)** in nuclear spreads of spermatocytes collected from 24-day-old mice. *Spo11*^{-/-} and *Syce2*^{-/-} *Spo11*^{-/-} spermatocytes are shown with cloud-like ATR **(a)** or TOPBP1 **(b)** accumulation, or with BRCA1 localized to axes **(c)** in γ H2AX-marked pseudo-sex bodies. In **a** and **b**, *Hormad1*^{-/-} *Spo11*^{-/-} cells are shown without a pseudo-sex body and without ATR or TOPBP1 accumulation on chromatin, respectively. In **c**, a *Hormad1*^{-/-} *Spo11*^{-/-} cell is shown with a pseudo-sex body, within which no BRCA1

termed the sex body^{57–59}. Efficient sex-chromosome silencing is essential for progression beyond mid-pachytene^{60,61}. In spermatocytes defective in DSB repair or synaptonemal-complex formation, ATR activity (γ H2AX) persists on unsynapsed autosomes, and fails to accumulate strongly on sex chromosomes^{8–12,60}. Consequently, sex-body formation and sex-chromosome silencing fail, resulting in mid-pachytene apoptosis^{60,61}. Sex-body formation is defective in *Hormad1*^{-/-} spermatocytes⁴¹ (Fig. 4a). Nevertheless, γ H2AX accumulated in chromatin regions that are not associated strongly with unsynapsed chromosome axes in *Hormad1*^{-/-} spermatocytes. This abnormal localization of γ H2AX may result from either lower DSB numbers and incomplete synaptonemal-complex formation or a more direct involvement of HORMAD1 in the recruitment of ATR activity to unsynapsed chromatin.

To test these two possibilities, we examined the effect of *Hormad1*^{-/-} mutation on the MSUC pathway in a *Spo11*^{-/-} background^{4,5}.

association with the axis was detected. Note that only a small number of *Hormad1*^{-/-} *Spo11*^{-/-} spermatocytes show pseudo-sex-body-like accumulation of γ H2AX (Fig. 4c). Scale bars, 10 μ m. **(d–f)** Frequency of cloud-like ATR **(d)** and TOPBP1 **(e)** accumulation and frequency of BRCA1 association with axes **(f)** in spermatocytes with fully formed chromosome axes. ATR- and TOPBP1-rich chromatin domains are frequently observed in *Spo11*^{-/-} and *Syce2*^{-/-} *Spo11*^{-/-} spermatocytes, and BRCA1 association with axes is also observed in these mutants. ATR and TOPBP1 are virtually absent from chromatin in most of the *Hormad1*^{-/-} *Spo11*^{-/-} cells, and BRCA1 localization to axes was never observed in *Hormad1*^{-/-} *Spo11*^{-/-} spermatocytes.

Although synaptonemal-complex formation is abnormal in *Spo11*^{-/-} spermatocytes, MSUC is active and a random subset of unsynapsed chromosome axes is frequently associated with one or a few γ H2AX-rich silenced chromatin domains termed pseudo-sex bodies^{12,50} (Fig. 4b). As synaptonemal-complex formation is severely compromised in *Hormad1*^{-/-} *Spo11*^{-/-} meiocytes, relative to *Spo11*^{-/-} mutants (Fig. 1), we controlled for loss of synaptonemal complexes by comparing pseudo-sex-body formation and the behaviour of MSUC proteins in the *Hormad1*^{-/-} *Spo11*^{-/-} double mutant with the *Syce2*^{-/-} *Spo11*^{-/-} double mutant, which lacks a synaptonemal-complex central-element component and does not form synaptonemal complexes⁹. The number of pseudo-sex-body-like chromatin domains formed is much lower in *Hormad1*^{-/-} *Spo11*^{-/-} double-mutant spermatocytes, relative to both *Spo11*^{-/-} and *Syce2*^{-/-} *Spo11*^{-/-} controls (Fig. 4b,c). Lack of HORMAD1 strongly reduces total nuclear γ H2AX immunofluorescence staining in the *Spo11*^{-/-} back-

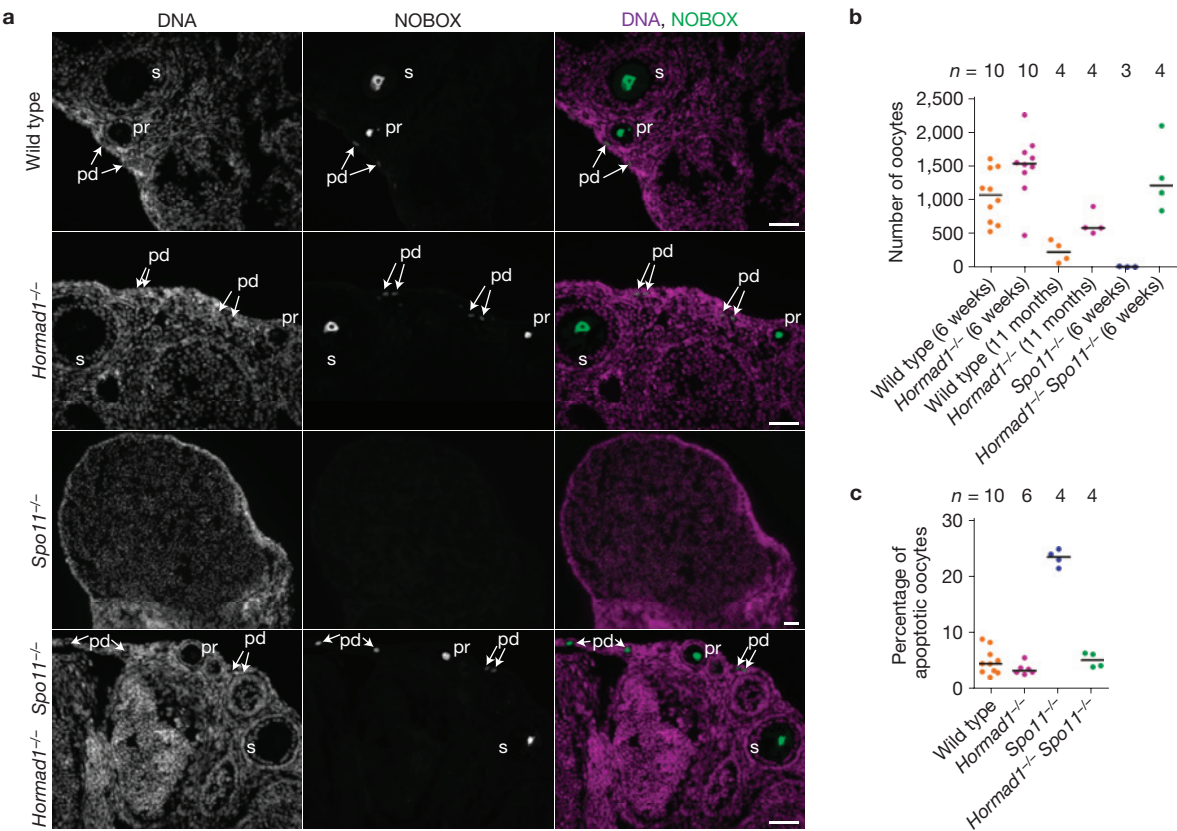


Figure 6 Lack of HORMAD1 allows survival of oocytes in the synaptonemal-complex-defective *Spo11*^{-/-} mutant. **(a)** NOBOX (postnatal oocyte marker) was detected by immunofluorescence microscopy on cryosections of ovaries from 6-week-old mice. DNA was detected by DAPI. Oocytes in primordial (pd), primary (pr) and secondary (s) follicular stages are shown in wild-type, *Hormad1*^{-/-} and *Hormad1*^{-/-} *Spo11*^{-/-} ovaries. In the synaptonemal-complex-defective *Spo11*^{-/-} mutant, oocyte

numbers are much lower. A lower-magnification section of a *Spo11*^{-/-} ovary is shown to better illustrate the absence of oocytes. Scale bars, 50 μm. **(b)** Sum of oocyte numbers on every tenth section of sectioned-through ovary pairs at the indicated ages. Each data point represents a mouse. **(c)** Fraction of apoptotic oocytes in the ovaries of 1-day-old (1 dpp) mice of indicated genotypes. Horizontal lines show medians in **b** and **c**.

ground, whereas loss of synaptonemal-complex formation does not (Fig. 4d). Both ATR and TOPBP1 accumulate within pseudo-sex bodies, and BRCA1 accumulates on chromosome axes associated with pseudo-sex bodies^{12,50,60} (Fig. 5). We observed lower levels of TOPBP1, ATR and BRCA1 localized to unsynapsed chromatin in the *Hormad1*^{-/-} *Spo11*^{-/-} double mutant when compared with both control strains (Fig. 5). This phenotype is probably not caused by an early block in meiotic progression, as *Spo11*^{-/-}, *Syce2*^{-/-} *Spo11*^{-/-} and *Hormad1*^{-/-} *Spo11*^{-/-} spermatocytes are eliminated in stage-IV tubules (Supplementary Fig. S6). The most straightforward interpretation is that HORMAD1 promotes recruitment of MSUC proteins to unsynapsed chromatin regions independently of its role in the formation of processed DSBs and synaptonemal complexes.

The prophase checkpoint is less well understood in oocytes than in spermatocytes, although ATR activation and MSUC have been implicated in the female checkpoint^{13,57}. In the absence of heterologous sex chromosomes, oocytes do not form sex bodies. Nevertheless, *Spo11*^{-/-} oocytes frequently contain male pseudo-sex-body-like γH2AX-rich chromatin domains that also contain TOPBP1 and BRCA1 (Supplementary Fig. S9; ref. 13). The number of such female ‘pseudo-sex bodies’ formed is much lower in *Hormad1*^{-/-} *Spo11*^{-/-} oocytes (Supplementary Fig. S9), indicating that HORMAD1 may have a role in MSUC and the prophase checkpoint in females.

Therefore, we compared the number of oocytes in ovaries from 6-week-old wild-type, *Hormad1*^{-/-}, *Spo11*^{-/-} and *Hormad1*^{-/-} *Spo11*^{-/-} animals and in ovaries from 11-month-old wild-type and *Hormad1*^{-/-} animals (Fig. 6a,b). In the synaptonemal-complex-defective *Spo11*^{-/-} mutant, very few oocytes survive until six weeks. Despite defective synaptonemal-complex formation, oocyte numbers are not lower in *Hormad1*^{-/-} (ref. 41) or *Hormad1*^{-/-} *Spo11*^{-/-} animals, relative to wild-type animals. Notably, oocyte apoptosis rates are similar in wild-type, *Hormad1*^{-/-} and *Hormad1*^{-/-} *Spo11*^{-/-} mice, and are greatly elevated in the *Spo11*^{-/-} mutant one day after birth, when many of the synaptonemal-complex-defective oocytes are eliminated (Fig. 6c). Thus, *Hormad1*^{-/-} suppresses oocyte loss in the *Spo11*^{-/-} background. These observations demonstrate that HORMAD1 is essential for the female prophase checkpoint that eliminates oocytes with abnormal synaptonemal-complex formation and homologue alignment.

Chromosome segregation in *Hormad1*^{-/-} oocytes

Follicular oocyte development does not require HORMAD1 (ref. 41) because we found oocytes at all stages of follicular development in *Hormad1*^{-/-} and *Hormad1*^{-/-} *Spo11*^{-/-} animals (Fig. 6a). This allowed us to test whether chiasmata form during the first meiotic metaphase in the absence of HORMAD1. On average, approximately one-third of chromosomes were connected by chiasmata in *in*

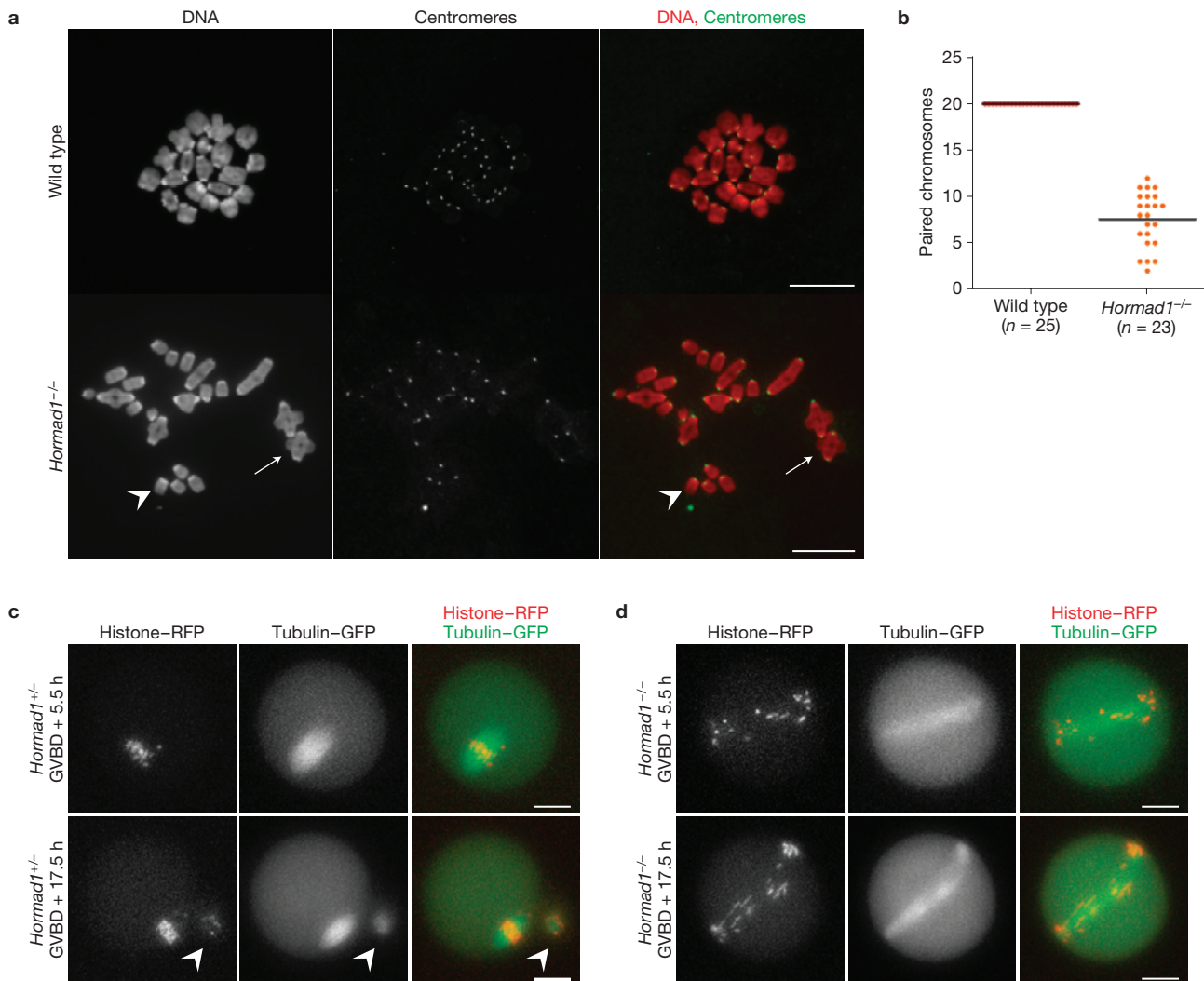


Figure 7 Lower numbers of chiasmata form in *Hormad1*^{-/-} oocytes. (a) Centromeres were detected by immunofluorescence microscopy and DNA was detected by propidium iodide staining on nuclear spreads of *in vitro*-matured metaphase stage oocytes. In wild-type cells, 20 pairs of chromosomes are connected by chiasmata. In the *Hormad1*^{-/-} mutant, many chromosomes do not have chiasmata (one such chromosome is marked by an arrowhead). Arrow marks a pair of chromosomes connected by a chiasma in the mutant oocyte. Note that bivalents are symmetrical and chiasmata form between chromosomes of identical length in the mutant, indicating that crossover formation took place between homologous chromosomes. Chromosomes scatter over a larger area during nuclear spreading in the mutant; therefore, it was not possible to include all 40 chromosomes of a meiosis I oocyte in the image. Scale bars, 10 μm. (b) The average numbers of paired chromosomes connected by chiasmata (marked by line) are nearly threefold lower in *in vitro*-matured

Hormad1^{-/-} oocytes, relative to wild-type oocytes. (c,d) mRNAs encoding β-tubulin-GFP and histone-H2B-RFP were injected into wild-type (c) and *Hormad1*^{-/-} (d) oocytes during the germinal vesicle stage (prophase), and the oocytes were matured *in vitro*. The fluorescent proteins in the oocytes were imaged 5.5 h after germinal vesicle break down (GVBD), at a time when wild-type oocytes are in the first meiotic metaphase, and 17.5 h after GVBD, at a time when wild-type oocytes are arrested in the second meiotic metaphase. A polar body (marked by arrowhead in c), which was extruded 7 h after GVBD (Supplementary Movie S1), is observed next to the metaphase II stage wild-type oocyte at the 17.5 h time point. In the *Hormad1*^{-/-} oocyte (d), the meiotic spindle is abnormally long and chromosomes fail to align at both time points. Meiotic anaphase did not take place in the *Hormad1*^{-/-} oocyte shown (Supplementary Movie S2), and no polar body can be observed at either time point (d). Scale bars, 20 μm.

in vitro-matured metaphase *Hormad1*^{-/-} oocytes, which corresponds well to the number of MLH1 foci observed in pachytene oocytes (Figs 2k and 7). Chiasmata formation depends both on sister-chromatid cohesion along chromosome arms and on crossover formation. Thus, our observations suggest that sister-chromatid cohesion is intact and that MLH1-marked DSB sites are efficiently resolved as crossovers in the *Hormad1*^{-/-} mutant.

We evaluated the consequences of lower crossover numbers on the first meiotic division in *in vitro*-matured oocytes. Although

nuclear-envelope-breakdown efficiency was similar in wild-type (142 of 149) and *Hormad1*^{-/-} (73 of 77) oocytes, the efficiency of polar-body extrusion was much lower in the mutant (5 of 60), relative to the wild-type (92 of 95) oocytes. Video microscopy shows that *Hormad1*^{-/-} oocytes have abnormally long meiosis I spindles, on which chromosomes fail to align (Fig. 7c,d and Supplementary Movies S1, S2). This defect probably causes anaphase failure and the polar-body-extrusion defect. Despite the abnormal first meiotic division, some of the *Hormad1*^{-/-} oocytes are fertilized *in vivo* because

in a few cases (3 of 11 breeding pairs) we found one to three reabsorbing embryos five to eight days after breeding began. Nevertheless, embryos never developed to full term in *Hormad1*^{-/-} females (19 females, 125 breeding weeks). Infertility and loss of embryos are consistent with the meiotic chromosome segregation defects (Fig. 7c,d and Supplementary Movies S1, S2) and with the reported widespread aneuploidy in early embryos in *Hormad1*^{-/-} females⁴¹.

DISCUSSION

We analysed the functions of HORMAD1 using mouse genetics. We propose three distinct biological functions for mouse HORMAD1. First, HORMAD1 increases the steady-state numbers of single-stranded DSB ends, thereby facilitating homology search. Our data suggest that HORMAD1 promotes efficient DSB formation or resection of DSB ends, or both. As budding-yeast Hop1 is required for efficient DSB formation^{29,35}, we favour the first possibility. In budding yeast, inter-homologue crossover numbers remain relatively stable when there are fewer DSBs, a phenomenon called crossover homeostasis⁶². A comparable reduction in the numbers of early-intermediate recombination protein foci (particularly RPA) and of chiasmata in the *Hormad1*^{-/-} mutant may be interpreted as a sign of lack of crossover homeostasis in mice (Figs 2 and 7). However, a trivial explanation is that crossover homeostasis can function only if homology search succeeds and homologues align. Hence, the approximately threefold reduction in crossover formation may simply reflect the low number of homologues that manage to partially or fully align in *Hormad1*^{-/-} meiocytes. The observed correlation between numbers of SYCP1 (synaptonemal complex protein 1) stretches and MLH1 foci in oocytes is consistent with this latter possibility (Fig. 2j). Our data suggest that *Hormad1*^{-/-} meiocytes are proficient in DSB repair steps that are important for homology search and inter-homologue crossover formation, and the lower level of crossover formation is caused by a reduction in the number of single-stranded DSB ends. Consistent with this hypothesis, some homologues seem to synapse at least partially in *Hormad1*^{-/-} meiocytes, a conclusion based on the observations that incomplete synaptonemal complexes form between chromosomes of similar axis length, and that synaptonemal-complex formation largely depends on SPO11-induced DSBs and presumably on the downstream process of homology search in *Hormad1*^{-/-} cells (Fig. 1 and Supplementary Fig. S5). Furthermore, chiasmata form between chromosomes of identical length, indicating that inter-homologue chiasmata, which are consequences of inter-homologue crossovers, form in *Hormad1*^{-/-} oocytes (Fig. 7a).

Second, HORMAD1 promotes synaptonemal-complex formation independently of its role in homology search. This conclusion is based on the observation that HORMAD1 is needed for efficient non-homologous synaptonemal-complex formation (Fig. 1 and Supplementary Fig. S5). It is possible that HORMAD1 is required only for pathological non-homologous synapsis. However, we consider it unlikely that as a prelude to homology search unsynapsed chromosome axes are loaded with a protein (HORMAD1) that specifically promotes non-homologous synapsis. It seems more likely that HORMAD1 promotes synaptonemal-complex formation between axes that come into close proximity, irrespective of underlying homology.

Finally, HORMAD1 plays a key role in the male mid-pachytene checkpoint and the female meiotic prophase checkpoint, both

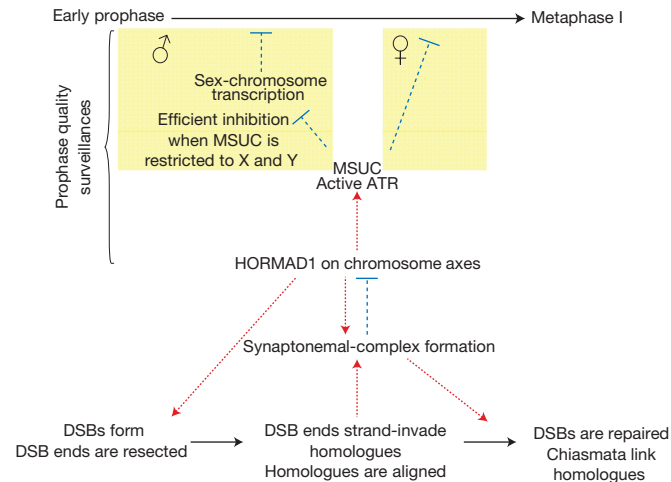


Figure 8 Model for meiotic progression: negative feedback loop of HORMAD1 and synaptonemal-complex coordinates homology search and meiotic progression. Processes, activation-promotion and inhibition are marked by solid black arrows, red dotted arrows and blue flat-ended dashed arrows, respectively. HORMAD1 associates with forming chromosome axes at the beginning of meiosis, where it promotes DSB formation and/or processing of DSBs. It thereby ensures that adequate numbers of single-stranded DSBs are available for homology search. As part of the homology search process, DSB ends strand-invade into homologues. Multiple strand-invasion events along the length of chromosomes lead to full alignment of pairs of homologues, which is a prerequisite for the completion of synaptonemal-complex formation. HORMAD1 also promotes synaptonemal-complex formation through a mechanism that is independent of homology search. Synaptonemal-complex formation leads to depletion of HORMAD1 from axes and downregulation of HORMAD1 function⁴⁰. Hence, in spermatocytes, full autosomal synaptonemal-complex formation leads to a restriction of HORMAD1 and ATR activity to sex chromosomes, thereby promoting efficient silencing of sex chromosomes, which is a prerequisite for progression beyond mid-pachytene^{13,60,61}. In oocytes, completion of synaptonemal-complex formation on all chromosomes leads to complete inactivation of HORMAD1, which in turn leads to downregulation of ATR and MSUC. As sustained ATR activity and/or sustained MSUC is believed to block progression beyond meiotic prophase¹³, full synaptonemal-complex formation and HORMAD1 inactivation link successful homologue alignment with progression beyond meiotic prophase. Note that successful DSB repair is probably also required for full downregulation of ATR activity and for meiotic progression in oocytes (for the sake of simplicity, this branch of the prophase checkpoint is not shown in the model).

of which eliminate meiocytes with defects in DSB repair and/or in homologue alignment and synaptonemal-complex formation. HORMAD1 is required for efficient build-up of ATR activity on unsynapsed chromosome regions, a process that is believed to form the basis of MSUC and meiotic prophase quality control in both sexes^{13,14,57} (Figs 4,5 and Supplementary Fig. S9). In males, mid-pachytene apoptosis of spermatocytes defective in DSB repair and synaptonemal-complex formation is triggered by failure of MSUC on sex chromosomes, allowing transcription of genes whose expression is incompatible with survival beyond mid-pachytene^{13,60,61}. In females, elimination of defective oocytes may be triggered by inappropriate MSUC or persistent ATR activity during prophase¹³. Therefore, the apparently opposite effect of *Hormad1* mutation in the two sexes (that is, apoptosis of spermatocytes and survival of synaptonemal-complex-defective oocytes) is probably caused by a common defect in recruitment of ATR activity to unsynapsed chromosomes. ATR is recruited to DSB sites in somatic cells, where it becomes active

as part of the G2/M DSB repair checkpoint¹⁴. In meiosis, ATR and its activators are recruited to both DSB sites and unsynapsed chromatin^{13,14,51–57,60}. Our data raise the possibility that HORMAD1 fulfils its role in meiotic progression control by recruiting ATR and/or other components of the somatic DSB checkpoint machinery to unsynapsed chromatin, thereby adapting their functions for the detection of unsynapsed chromosome axes.

A comprehensive model for meiotic progression control emerges from this study and previous work showing that HORMAD1 is depleted from chromosome axes in response to synaptonemal-complex formation⁴⁰ (Fig. 8). We propose that the synaptonemal complex and HORMAD1 interact in a negative feedback loop, to coordinate meiotic progression with successful homologue alignment. HORMAD1 promotes homologue alignment and synaptonemal-complex formation. In turn, synaptonemal-complex formation downregulates HORMAD1 function by promoting HORMAD1 depletion from aligned homologues, which is a prerequisite for progression beyond the first meiotic prophase.

Although our observations and consistent observations of others⁴¹ clearly show the importance of HORMAD1 during meiosis in mice, *Hormad1*^{-/-} phenotypes seem partial. It is possible that HORMAD2 partially substitutes for its parologue HORMAD1 during meiosis, and analysis of *Hormad1*^{-/-} *Hormad2*^{-/-} mice, once this mutant is available, will determine whether this is the case. □

METHODS

Methods and any associated references are available in the online version of the paper at <http://www.nature.com/naturecellbiology/>

Note: Supplementary Information is available on the Nature Cell Biology website

ACKNOWLEDGEMENTS

We thank A. Hientzsch and K. Duerschke for general laboratory support and technical assistance; R. Jessberger for sharing ideas, antibodies (anti-SYCP3, anti-STAG3 and anti-SMC3) and support; F. Baudat and B. De Massy for providing us with Spo11^{+/−} mice; J. Chen for the anti-TOPBP1 antibody; E. Marcon for the anti-RPA antibody; C. Höög for anti-SYCE1 and anti-SYCE2 antibodies; G.C. Enders for the anti-GCNA antibody; and M.P. Thelen for the anti-SPO11 antibody. We are grateful to M. Siomos and D. Knapp for discussion, revising and proofreading the manuscript. The Deutsche Forschungsgemeinschaft (DFG; grants: TO421/4-1 SPP1384 and TO421/3-1) and the Sächsisches Staatsministerium für Wissenschaft und Kunst supported K.D. and A.T.; Grants HD53855 and HD40916 from the US National Institutes of Health supported J.L., I.R., M.J. and S.K.; ARC (Subvention fixe 1143) and La Ligue Regionale (RS09/75-39) supported K.H. and K.W.; the Medical Research Council UK supported H.J.C.; the DFG research centre and cluster of excellence to the Center for Regenerative Therapies Dresden (CRTD) supported the work of K.A.; a CRTD seed grant supported K.A. and A.T.; and an EFRE grant (Europäischer Fonds für Regionale Entwicklung) supported K.A., J.F. and A.F.S.

AUTHOR CONTRIBUTIONS

K.D. designed, carried out and analysed most of the experiments; J.L., I.R., M.J. and S.K. contributed with SPO11-oligonucleotide measurements; J.F., K.A. and A.F.S. designed and generated the targeting construct and targeted embryonic stem cells; K.H. and K.W. carried out oocyte-maturation experiments and oocyte video microscopy; H.J.C. provided the *Syce2*^{+/−} mouse, A.T. was involved in oocyte-maturation experiments and oocyte counts, helped K.D. in experimental design and wrote the paper together with K.D. All authors were involved in discussions and commented on the manuscript.

COMPETING FINANCIAL INTERESTS

The authors declare no competing financial interests.

Published online at <http://www.nature.com/naturecellbiology/>

Reprints and permissions information is available online at <http://npg.nature.com/reprintsandpermissions/>

- Baudat, F. & de Massy, B. Regulating double-stranded DNA break repair towards crossover or non-crossover during mammalian meiosis. *Chromosome Res.* **15**, 565–577 (2007).
- Hunter, N. *Meiotic Recombination in Molecular Genetics of Recombination* (Springer, 2007).
- Keeney, S., Giroux, C. N. & Kleckner, N. Meiosis-specific DNA double-strand breaks are catalyzed by Spo11, a member of a widely conserved protein family. *Cell* **88**, 375–384 (1997).
- Baudat, F., Manova, K., Yuen, J. P., Jasin, M. & Keeney, S. Chromosome synapsis defects and sexually dimorphic meiotic progression in mice lacking Spo11. *Mol. Cell* **6**, 989–998 (2000).
- Romanienko, P. J. & Camerini-Otero, R. D. The mouse *Spo11* gene is required for meiotic chromosome synapsis. *Mol. Cell* **6**, 975–987 (2000).
- Sun, H., Treco, D. & Szostak, J. W. Extensive 3'-overhanging, single-stranded DNA associated with the meiosis-specific double-strand breaks at the ARG4 recombination initiation site. *Cell* **64**, 1155–1161 (1991).
- Hamer, G., Novak, I., Kouzenetsova, A. & Höög, C. Disruption of pairing and synapsis of chromosomes causes stage-specific apoptosis of male meiotic cells. *Theriogenology* **69**, 333–339 (2008).
- Hamer, G. *et al.* Progression of meiotic recombination requires structural maturation of the central element of the synaptonemal complex. *J. Cell Sci.* **121**, 2445–2451 (2008).
- Bolcun-Filas, E. *et al.* SYCE2 is required for synaptonemal complex assembly, double strand break repair, and homologous recombination. *J. Cell Biol.* **176**, 741–747 (2007).
- Bolcun-Filas, E. *et al.* Mutation of the mouse *Syce1* gene disrupts synapsis and suggests a link between synaptonemal complex structural components and DNA repair. *PLoS Genet.* **5**, e1000393 (2009).
- de Vries, F. A. *et al.* Mouse *Sycp1* functions in synaptonemal complex assembly, meiotic recombination, and XY body formation. *Genes Dev.* **19**, 1376–1389 (2005).
- Barchi, M. *et al.* Surveillance of different recombination defects in mouse spermatocytes yields distinct responses despite elimination at an identical developmental stage. *Mol. Cell Biol.* **25**, 7203–7215 (2005).
- Burgoyne, P. S., Mahadevaiah, S. K. & Turner, J. M. The consequences of asynapsis for mammalian meiosis. *Nat. Rev. Genet.* **10**, 207–216 (2009).
- Burgoyne, P. S., Mahadevaiah, S. K. & Turner, J. M. The management of DNA double-strand breaks in mitotic G2, and in mammalian meiosis viewed from a mitotic G2 perspective. *Bioessays* **29**, 974–986 (2007).
- Aravind, L. & Koonin, E. V. The HORMA domain: a common structural denominator in mitotic checkpoints, chromosome synapsis and DNA repair. *Trends Biochem. Sci.* **23**, 284–286 (1998).
- Martinez-Perez, E. & Villeneuve, A. M. HTP-1-dependent constraints coordinate homolog pairing and synapsis and promote chiasma formation during *C. elegans* meiosis. *Genes Dev.* **19**, 2727–2743 (2005).
- Nonomura, K., Nakano, M., Eiguchi, M., Suzuki, T. & Kurata, N. PAIR2 is essential for homologous chromosome synapsis in rice meiosis I. *J. Cell Sci.* **119**, 217–225 (2006).
- Couteau, F. & Zetka, M. HTP-1 coordinates synaptonemal complex assembly with homolog alignment during meiosis in *C. elegans*. *Genes Dev.* **19**, 2744–2756 (2005).
- Goodyer, W. *et al.* HTP-3 links DSB formation with homolog pairing and crossing over during *C. elegans* meiosis. *Dev. Cell* **14**, 263–274 (2008).
- Martinez-Perez, E. *et al.* Crossovers trigger a remodeling of meiotic chromosome axis composition that is linked to two-step loss of sister chromatid cohesion. *Genes Dev.* **22**, 2886–2901 (2008).
- Severson, A. F., Ling, L., van Zuylen, V. & Meyer, B. J. The axial element protein HTP-3 promotes cohesin loading and meiotic axis assembly in *C. elegans* to implement the meiotic program of chromosome segregation. *Genes Dev.* **23**, 1763–1778 (2009).
- Zetka, M. C., Kawasaki, I., Strome, S. & Muller, F. Synapsis and chiasma formation in *Caenorhabditis elegans* require HIM-3, a meiotic chromosome core component that functions in chromosome segregation. *Genes Dev.* **13**, 2258–2270 (1999).
- Couteau, F., Nabeshima, K., Villeneuve, A. & Zetka, M. A component of *C. elegans* meiotic chromosome axes at the interface of homolog alignment, synapsis, nuclear reorganization, and recombination. *Curr. Biol.* **14**, 585–592 (2004).
- MacQueen, A. J., Colaiacovo, M. P., McDonald, K. & Villeneuve, A. M. Synapsis-dependent and -independent mechanisms stabilize homolog pairing during meiotic prophase in *C. elegans*. *Genes Dev.* **16**, 2428–2442 (2002).
- Nabeshima, K., Villeneuve, A. M. & Hillers, K. J. Chromosome-wide regulation of meiotic crossover formation in *Caenorhabditis elegans* requires properly assembled chromosome axes. *Genetics* **168**, 1275–1292 (2004).
- Sanchez-Moran, E., Santos, J. L., Jones, G. H. & Franklin, F. C. ASY1 mediates AtDMC1-dependent interhomolog recombination during meiosis in *Arabidopsis*. *Genes Dev.* **21**, 2220–2233 (2007).
- Hollingsworth, N. M. & Byers, B. *HOP1*: a yeast meiotic pairing gene. *Genetics* **121**, 445–462 (1989).
- Loidl, J., Klein, F. & Scherthan, H. Homologous pairing is reduced but not abolished in asynaptic mutants of yeast. *J. Cell Biol.* **125**, 1191–1200 (1994).
- Schwacha, A. & Kleckner, N. Identification of joint molecules that form frequently between homologs but rarely between sister chromatids during yeast meiosis. *Cell* **76**, 51–63 (1994).

30. Hollingsworth, N. M. & Ponte, L. Genetic interactions between HOP1, RED1 and MEK1 suggest that MEK1 regulates assembly of axial element components during meiosis in the yeast *Saccharomyces cerevisiae*. *Genetics* **147**, 33–42 (1997).
31. Bailis, J. M., Smith, A. V. & Roeder, G. S. Bypass of a meiotic checkpoint by overproduction of meiotic chromosomal proteins. *Mol. Cell Biol.* **20**, 4838–4848 (2000).
32. Woltering, D. *et al.* Meiotic segregation, synapsis, and recombination checkpoint functions require physical interaction between the chromosomal proteins Red1p and Hop1p. *Mol. Cell Biol.* **20**, 6646–6658 (2000).
33. Niu, H. *et al.* Partner choice during meiosis is regulated by Hop1-promoted dimerization of Mek1. *Mol. Biol. Cell* **16**, 5804–5818 (2005).
34. Niu, H. *et al.* Mek1 kinase is regulated to suppress double-strand break repair between sister chromatids during budding yeast meiosis. *Mol. Cell Biol.* **27**, 5456–5467 (2007).
35. Carballo, J. A., Johnson, A. L., Sedgwick, S. G. & Cha, R. S. Phosphorylation of the axial element protein Hop1 by Mec1/Tel1 ensures meiotic interhomolog recombination. *Cell* **132**, 758–770 (2008).
36. Joshi, N., Barot, A., Jamison, C. & Borner, G. V. Pch2 links chromosome axis remodeling at future crossover sites and crossover distribution during yeast meiosis. *PLoS Genet.* **5**, e1000557 (2009).
37. Zetka, M. Homologue pairing, recombination and segregation in *Caenorhabditis elegans*. *Genome Dyn.* **5**, 43–55 (2009).
38. Hayashi, M., Chin, G. M. & Villeneuve, A. M. *C. elegans* germ cells switch between distinct modes of double-strand break repair during meiotic prophase progression. *PLoS Genet.* **3**, e191 (2007).
39. Fukuda, T., Daniel, K., Wojtasz, L., Toth, A. & Höög, C. A novel mammalian HORMA domain-containing protein, HORMAD1, preferentially associates with unsynapsed meiotic chromosomes. *Exp. Cell Res.* **316**, 158–171 (2010).
40. Wojtasz, L. *et al.* Mouse HORMAD1 and HORMAD2, two conserved meiotic chromosomal proteins, are depleted from synapsed chromosome axes with the help of TRIP13 AAA-ATPase. *PLoS Genet.* **5**, e1000702 (2009).
41. Shin, Y. H. *et al.* Hormad1 mutation disrupts synaptonemal complex formation, recombination, and chromosome segregation in mammalian meiosis. *PLoS Genet.* **6**, e1001190 (2010).
42. Ahmed, E. A. & de Rooij, D. G. Staging of mouse seminiferous tubule cross-sections. *Methods Mol. Biol.* **558**, 263–277 (2009).
43. Pittman, D. L. *et al.* Meiotic prophase arrest with failure of chromosome synapsis in mice deficient for *Dmc1*, a germline-specific RecA homolog. *Mol. Cell* **1**, 697–705 (1998).
44. Yoshida, K. *et al.* The mouse *RecA*-like gene *Dmc1* is required for homologous chromosome synapsis during meiosis. *Mol. Cell* **1**, 707–718 (1998).
45. Neale, M. J., Pan, J. & Keeney, S. Endonucleolytic processing of covalent protein-linked DNA double-strand breaks. *Nature* **436**, 1053–1057 (2005).
46. Moens, P. B., Marcon, E., Shore, J. S., Kochakpour, N. & Spyropoulos, B. Initiation and resolution of interhomolog connections: crossover and non-crossover sites along mouse synaptonemal complexes. *J. Cell Sci.* **120**, 1017–1027 (2007).
47. Baker, S. M. *et al.* Involvement of mouse Mlh1 in DNA mismatch repair and meiotic crossing over. *Nat. Genet.* **13**, 336–342 (1996).
48. Marcon, E. & Moens, P. MLH1p and MLH3p localize to precocious chiasmata of okadaic-acid-treated mouse spermatocytes. *Genetics* **165**, 2283–2287 (2003).
49. Fernandez-Capetillo, O., Liebe, B., Scherthan, H. & Nussenzweig, A. H2AX regulates meiotic telomere clustering. *J. Cell Biol.* **163**, 15–20 (2003).
50. Bellani, M. A., Romanienko, P. J., Cairatti, D. A. & Camerini-Otero, R. D. Spo11 is required for sex-body formation, and *Spo11* heterozygosity rescues the prophase arrest of *Atm*^{−/−} spermatocytes. *J. Cell Sci.* **118**, 3233–3245 (2005).
51. Moens, P. B. *et al.* The association of ATR protein with mouse meiotic chromosome cores. *Chromosoma* **108**, 95–102 (1999).
52. Plug, A. W. *et al.* Changes in protein composition of meiotic nodules during mammalian meiosis. *J. Cell Sci.* **111** (Pt 4), 413–423 (1998).
53. Plug, A. W. *et al.* ATM and RPA in meiotic chromosome synapsis and recombination. *Nat. Genet.* **17**, 457–461 (1997).
54. Keegan, K. S. *et al.* The Atr and Atm protein kinases associate with different sites along meiotically pairing chromosomes. *Genes Dev.* **10**, 2423–2437 (1996).
55. Perera, D. *et al.* TopBP1 and ATR colocalization at meiotic chromosomes: role of TopBP1/Cut5 in the meiotic recombination checkpoint. *Mol. Biol. Cell* **15**, 1568–1579 (2004).
56. Turner, J. M. *et al.* BRCA1, histone H2AX phosphorylation, and male meiotic sex chromosome inactivation. *Curr. Biol.* **14**, 2135–2142 (2004).
57. Turner, J. M. *et al.* Silencing of unsynapsed meiotic chromosomes in the mouse. *Nat. Genet.* **37**, 41–47 (2005).
58. Baarends, W. M. *et al.* Silencing of unpaired chromatin and histone H2A ubiquitination in mammalian meiosis. *Mol. Cell Biol.* **25**, 1041–1053 (2005).
59. Turner, J. M., Mahadevaiah, S. K., Ellis, P. J., Mitchell, M. J. & Burgoyne, P. S. Pachytene asynapsis drives meiotic sex chromosome inactivation and leads to substantial postmeiotic repression in spermatids. *Dev. Cell* **10**, 521–529 (2006).
60. Mahadevaiah, S. K. *et al.* Extensive meiotic asynapsis in mice antagonises meiotic silencing of unsynapsed chromatin and consequently disrupts meiotic sex chromosome inactivation. *J. Cell Biol.* **182**, 263–276 (2008).
61. Royo, H. *et al.* Evidence that meiotic sex chromosome inactivation is essential for male fertility. *Curr. Biol.* **20**, 2117–2123 (2010).
62. Martini, E., Diaz, R. L., Hunter, N. & Keeney, S. Crossover homeostasis in yeast meiosis. *Cell* **126**, 285–295 (2006).

METHODS

Hormad1 targeting. The *Hormad1*-targeting construct was designed according to the multi-purpose allele strategy⁶³. The splice-acceptor (SA)-IRES-LacZneo-pA and PGK-Blasticidin-pA cassettes flanked by *FRT* sites were inserted in intron 3 (Supplementary Fig. S2). The frame-shifting exon 4 was flanked by *loxP* sites. Plasmids were constructed using recombination methods⁶⁴. To modify the *Hormad1* locus, mouse R1 embryonic stem cells were cultured (using mitomycin-C-inactivated mouse embryonic fibroblasts as feeders) and electroporated with the linearized targeting constructs using standard protocols. Southern blotting was used to identify correctly targeted embryonic stem cell clones: DNA was digested overnight with *Bcl*I, *Bsu*36I or *Hind*III for Southern blots with an internal-, 5'- or 3'-probe, respectively, and DNA fragments were separated on 0.8% agarose gels (data not shown).

Generation of knockouts and genotyping. We generated mice that carried either of two different *Hormad1*-null alleles (*Hormad1*^{insertion} and *Hormad1*^{deletion}) or an allele with restored functionality (*Hormad1*^{restored}; Supplementary Fig. S2). Two independent embryonic stem cell clones with a single integration of the targeting construct into the *Hormad1* locus were used to generate chimeric animals. Progeny of the chimeric animals crossed with C57BL/6OlaHsd females were genotyped by Southern blotting and PCR (Supplementary Fig. S2). In subsequent crosses, only PCR was used for genotyping the various alleles of *Hormad1* from tail-tip DNA. Genotyping primers: LacZ forward 5'-TGGCTTCGCTACCTGGAGAGAC, LacZ reverse 5'-AATCACCGCCGTAAGCCGACAC, 5loxD 5'-TCCCTTCTGTCTCCCCATCT-CC, loxP1 5'-GCTATACGAAGTTATAAGCCGAC, 3loxD 5'-TGGGTGCAAGCC-TTAAATCCC. PCR product sizes with LacZ-forward/LacZ-reverse primers: *Hormad1*^{insertion} template—208 bp, other alleles—no specific product; with LoxP1/3loxD primers: *Hormad1*^{insertion}, *Hormad1*^{restored} and *Hormad1*^{deletion} templates—267 bp, wild-type allele—no specific product; with 5loxD/3loxD primers: *Hormad1*^{insertion} and *Hormad1*^{restored} templates—487 bp, wild-type allele—377 bp, *Hormad1*^{deletion} allele—no specific product. To generate *Hormad1*^{restored} /+ mice, we crossed ES26-derived *Hormad1*^{insertion} /+ mice with hACTB:FLPe transgenic mice⁶⁵. To generate *Hormad1*^{deletion} /+ mice, we crossed *Hormad1*^{restored} /+ with PGK-Cre transgenic mice⁶⁶.

Animal experiments. *Dmc1*-, *Spo11*- or *Syce2*-knockout mice were reported earlier^{4,9,43}. Experiments were carried out in a mixed background (with 75–87.5% contribution from the C57BL/6OlaHsd inbred line). Whenever possible, experimental animals were compared with littermate controls or with age-matched non-littermate controls from the same colony. Although some of the figures show data from juveniles, all of our conclusions were reconfirmed from adult mice (more than 8 weeks old). In Fig. 2e–h, data points from different ages (16 days and 8 weeks) were pooled when wild-type and *Hormad1*^{+/−} littermates were compared, because data at different ages were similar in respect of averages and ranges. HORMAD1 is not detected by western blotting in *Hormad1*^{insertion/insertion} testis extract (Supplementary Fig. S2) and HORMAD1 is not detected by immunofluorescence microscopy on chromosome axes of *Hormad1*^{insertion/insertion} meiocytes (data not shown), indicating that *Hormad1*^{insertion} is a null allele. All of our conclusions are based on experiments that were carried out at least once in the ES26 *Hormad1*^{insertion} lineage. Apart from the kinetic analysis of axis and synaptonemal-complex formation, all of our conclusions involving experiments with single-knockout mice were reconfirmed in the ES21 *Hormad1*^{insertion} and ES26 *Hormad1*^{deletion} lineages. The phenotypes of ES26 *Hormad1*^{insertion/insertion}, ES21 *Hormad1*^{insertion/insertion} and ES26 *Hormad1*^{deletion/deletion} are indistinguishable. Therefore, we do not distinguish between *Hormad1*^{insertion} and *Hormad1*^{deletion} alleles, and we refer to them as the *Hormad1* allele. ES26 *Hormad1*^{restored/restored} mice are fertile. Testis size and synaptonemal-complex formation in spermatocytes are indistinguishable in *Hormad1*^{restored/restored} and wild-type mice (data not shown), which reconfirms that the phenotypes of *Hormad1*^{insertion/insertion} and *Hormad1*^{deletion/deletion} animals are caused by interference with production of wild-type *Hormad1* transcripts. For staging embryonic development, the day of detection of a vaginal plug was marked as 0.5 days post-coitum (dpc). All animals were used and maintained according to regulations provided by the animal ethics committee of the Technische Universität Dresden.

Immunofluorescence microscopy. Preparation and immunostaining of testis and ovary cryosections and nuclear surface spreads of meiocytes were carried out as described previously with a few modifications^{40,67}. Ovaries and testes were fixed for 25 and 40 min, respectively, in 3.6% formaldehyde buffered with 100 mM sodium phosphate at pH 7.4. Tissue sections with a thickness of 8 µm (ovary) or 7 µm (testis) were cut from frozen specimens embedded in O.C.T. (Sakura Finetek Europe). Sections dried onto slides were immunostained following washes in PBS at pH 7.4 and PBS at pH 7.4, with 0.1% Triton X-100. An assay that allows detection of TdT-mediated dUTP nick end labelling by immunofluorescence (IF-TUNEL) was carried out with an ApopTag Plus In Situ Apoptosis Fluorescein Detection Kit

(S 7111; Millipore). Antibodies were as described previously⁴⁰: rabbit anti-SMC3 (1:200) and rabbit anti-STAG3 (1:500, gifts from R. Jessberger, TUD, Dresden, Germany), guinea pig anti-SYCE1 (1:500) and guinea pig anti-SYCE2 (1:200, gifts from C. Höög, Karolinska Institute, Stockholm, Sweden), rabbit anti-RAD51 (1:200, Santa Cruz: sc-8349), rabbit anti-DMC1 (1:50, Santa Cruz: sc-22768), rabbit anti-MSH4 (1:150, Abcam: ab58666), mouse anti-MLH1 (1:50, BD Biosciences: 551092), rabbit anti-ATR (1:300, Calbiochem: PC538), goat anti-BRCA1 (1:30, Santa Cruz: sc-1553), rabbit anti-NOBOX (1:500, Abcam: ab41521), rat IgM anti-GCNA1 (ref. 68; 1:5, gift from G. C. Enders, The University of Kansas, Kansas City, USA), rabbit anti-cleaved PARP (Asp214; 1:250, Cell Signalling: 9544) and CREST human centromere auto-antibody HCT-100 (1:50, Cellon SA). For quantification of the γH2AX signal in spread spermatocytes (Fig. 4d), matched-exposure images were taken as described previously⁴⁰. We measured the total immunofluorescence signal intensity of γH2AX with ImageJ in squares that covered spread nuclei identified by 4,6-diamidino-2-phenylindole (DAPI) staining. Signal intensities were measured in four regions around the examined nuclei to estimate the background. The signal intensity values in Fig. 4d are background-corrected. To compare oocyte numbers in adults, we sectioned both ovaries of each mouse (8-µm-thick sections), identified oocytes by anti-NOBOX (oocyte marker⁶⁸) immunostaining and counted oocytes in every tenth section. To measure the rate of apoptosis in ovaries of 1 dpp animals, we sectioned both ovaries of each animal (8-µm-thick sections). The sections were stained for GCNA1 (oocyte marker⁶⁸) and for cleaved PARP1 (apoptosis marker). The numbers of cleaved PARP-positive and -negative oocytes were counted on every eighth section.

Staging meiotic prophase. First, we compared axis development and synaptonemal-complex formation in wild-type nuclear spreads to determine the stages of axis development corresponding to prophase stages. Thereafter, nuclear spreads were staged on the basis of axis development (see details in the legend of Supplementary Fig. S4).

Statistics. Statistical analysis was carried out with GraphPad Prism5 and SPSS 11.5 for Windows. For the comparison of independent samples, the two-tailed non-parametric Wilcoxon–Mann–Whitney two-sample rank-sum test was used.

Measurement of SPO11–oligonucleotide complexes and testis extracts. Immunoprecipitations of SPO11 and SPO11–oligonucleotide detection were carried out as published previously with minor modifications⁴⁵. Both testes from one juvenile or adult mouse were used for each experiment. Testes were decapsulated, then lysed in 800 µl lysis buffer (1% Triton X-100, 400 mM NaCl, 25 mM HEPES–NaOH at pH 7.4 and 5 mM EDTA). Lysates were centrifuged at 100,000 r.p.m. (355,040g) for 25 min in a TLA100.2 rotor. Supernatants were incubated with anti-mSPO11 antibody 180 (5 µg per pair of testes) at 4 °C for 1 h, followed by the addition of 30–40 µl protein-A–agarose beads (Roche) and incubation for another 3 h. Beads were washed three times with IP buffer (1% Triton X-100, 150 mM NaCl and 15 mM Tris–HCl at pH 8.0). Immunoprecipitates were eluted with Laemmli sample buffer and diluted sixfold to sevenfold in IP buffer. Eluates were incubated with anti-mSPO11 antibody 180 at 4 °C for 1 h, followed by the addition of 30–40 µl protein-A–agarose beads (Roche) and incubation overnight. Beads were washed three times with IP buffer and twice with buffer NEB4. SPO11–oligonucleotides were radiolabelled at 37 °C for 1 h using terminal deoxynucleotidyl transferase (Fermentas) and [α -³²P]dCTP. Beads were washed three times with IP buffer, boiled in Laemmli sample buffer and fractionated on 8% SDS-PAGE. Immunoprecipitates were transferred to a polyvinylidene fluoride membrane by semi-dry transfer (Bio-Rad). Radiolabelled species were detected and quantified with Fuji phosphor screens and ImageGuage software. The quantified signal shown on the figures is background-corrected; that is, the signal found in the *Spo11*^{+/−} testes was subtracted (Fig. 3a,c). To calculate the ratios of testes-weight-normalized SPO11–oligonucleotide levels, the background-corrected signal was divided by the weight of the testes. For western blot analysis, membranes were probed with anti-mSPO11 antibody 180 (1:2,000 in PBS containing 0.1% Tween 20 and 5% non-fat dry milk), then horseradish-peroxidase-conjugated protein A (Abcam; 1:10,000 in PBS containing 0.1% Tween 20 and 5% non-fat dry milk), and SPO11 was detected using the ECL+ reagent (GE Healthcare). The anti-SPO11 antibody was produced by the hybridoma cell line 180, which was generated by M.P. Thelen at Lawrence Livermore National Laboratory, California.

For anti-HORMAD1 western blot analysis (Supplementary Fig. S2), total testis extracts were prepared by boiling resuspended testes in Laemmli buffer. Standard methods were used for SDS-PAGE and immunoblotting.

In vitro culture and video microscopy of oocytes. Oocytes were collected from antral follicles of 9–16-week-old mice and placed in M2 medium (38 °C) supplemented with 100 µg ml^{−1} dibutyryl cyclic AMP (dbcAMP), which arrested oocytes in the germinal vesicle stage. Oocytes were induced to undergo meiotic maturation by rinsing and culture in M2 medium without dbcAMP (ref. 70). Only

oocytes in which germinal-vesicle breakdown (GVBD) was observed within 90 min after release were used for further experiments. Extrusion of the first polar body was determined by visual observation with light microscopy after overnight incubation (approximately 15–19 h after GVBD).

Video microscopy was carried out following injection of germinal vesicle oocytes with *in vitro*-transcribed mRNAs (Ambion mMessage mMachine kit) coding for histone-H2B fused to red fluorescent protein (RFP) and β -tubulin fused to green fluorescent protein (GFP; ref. 70). Movies were made on a Nikon TE2000E microscope with PrecisExite High Power LED Fluorescence (LAM 1: 400/465, LAM2: 585), equipped with a temperature chamber (Life Imaging Services), a Märzhäuser Scanning Stage and a CoolSNAP HQ2 camera, and controlled by Metamorph software. Acquisitions (8 z sections, every 2 μ m, Plan APO $\times 20/0.75$ NA objective) were obtained every 30 min, starting from GVBD + 5.5 h. GFP was set to 3% intensity, with an exposure time of 20 ms. RFP was set to 5% intensity, with a 15 ms exposure time.

63. Testa, G. *et al.* A reliable lacZ expression reporter cassette for multipurpose, knockout-first alleles. *Genesis* **38**, 151–158 (2004).

64. Zhang, Y., Buchholz, F., Muyrers, J. P. & Stewart, A. F. A new logic for DNA engineering using recombination in *Escherichia coli*. *Nat. Genet.* **20**, 123–128 (1998).
65. Rodriguez, C. I. *et al.* High-efficiency deleter mice show that FLPe is an alternative to Cre-loxP. *Nat. Genet.* **25**, 139–140 (2000).
66. Lallemand, Y., Luria, V., Haffner-Krausz, R. & Lonai, P. Maternally expressed PGK-Cre transgene as a tool for early and uniform activation of the Cre site-specific recombinase. *Transgenic Res.* **7**, 105–112 (1998).
67. Hodges, C. A. & Hunt, P. A. Simultaneous analysis of chromosomes and chromosome-associated proteins in mammalian oocytes and embryos. *Chromosoma* **111**, 165–169 (2002).
68. Enders, G. C. May J. J. 2nd developmentally regulated expression of a mouse germ cell nuclear antigen examined from embryonic day 11 to adult in male and female mice. *Dev. Biol.* **163**, 331–340 (1994).
69. Suzumori, N., Yan, C., Matzuk, M. M. & Rajkovic, A. Nobox is a homeobox-encoding gene preferentially expressed in primordial and growing oocytes. *Mech. Dev.* **111**, 137–141 (2002).
70. Niault, T. *et al.* Changing Mad2 levels affects chromosome segregation and spindle assembly checkpoint control in female mouse meiosis I. *PLoS One* **2**, e1165 (2007).

DOI: 10.1038/ncb2213

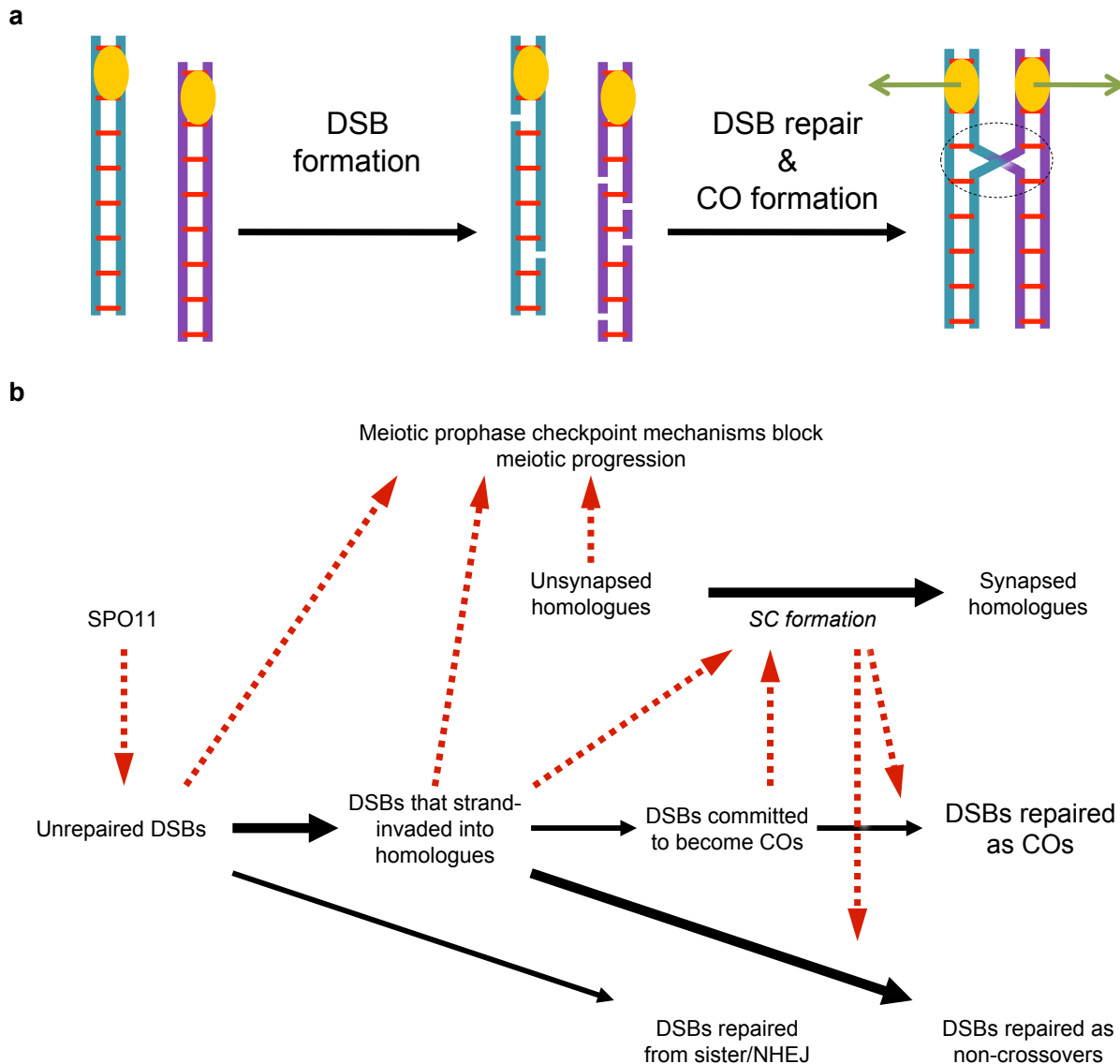
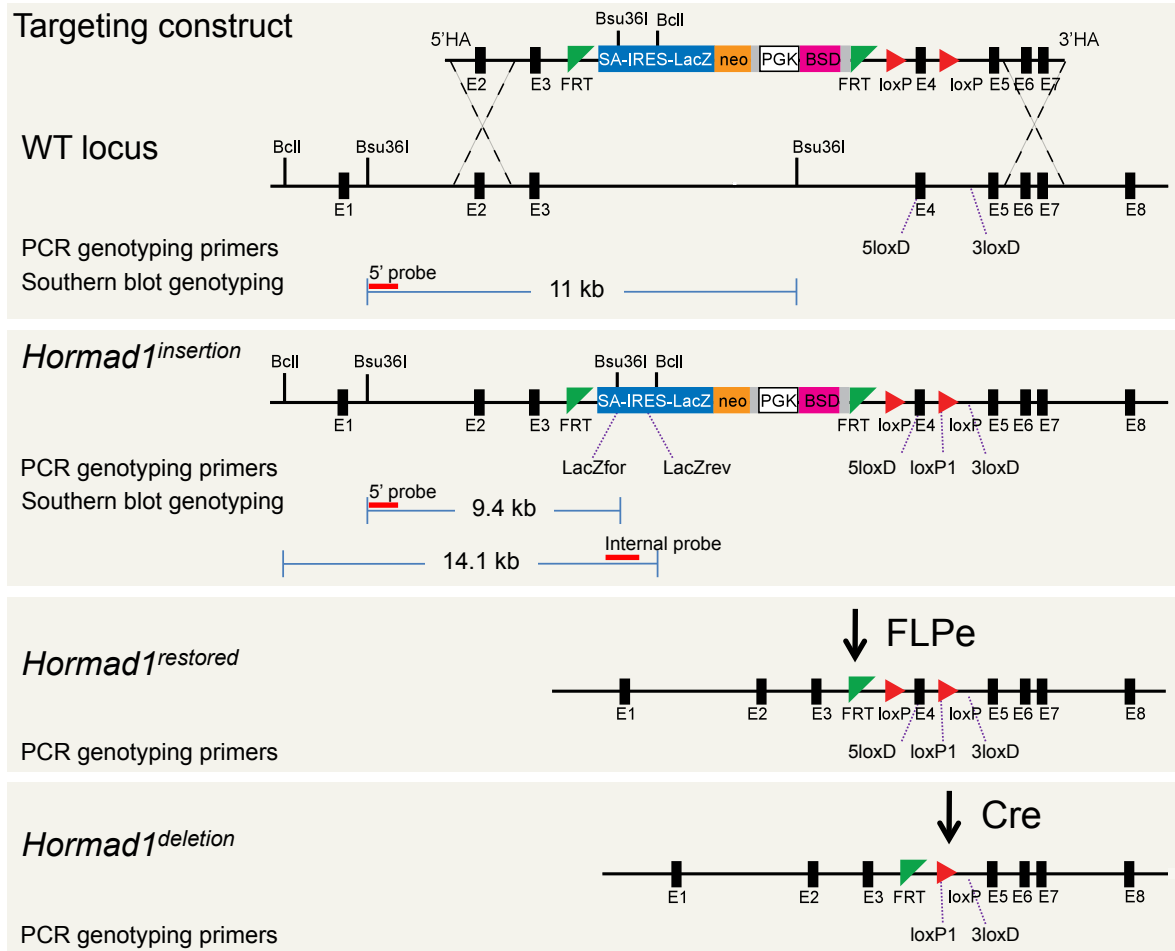


Figure S1 Schematic model for meiotic crossover formation in mammals (based on previously reviewed meiotic studies in mice and budding yeast^{1, 2, 13, 14}). **a**, Following replication, double-strand breaks (DSBs) are introduced into chromosomes that consist of two sister chromatids (cobalt and lilac vertical bars) held together by cohesion (red horizontal bars). Repair of DSBs results in at least one reciprocal exchange-crossover (CO) between homologous (non-sister) chromatids of each homologue pair, although most DSBs are repaired without CO formation. Sister chromatid cohesion and COs between homologues provide physical linkages that are visible as chiasmata (in dashed circle). Physical linkages between homologues facilitate the attachment of homologous kinetochores (yellow disks) to microtubules (green arrows) emanating from the opposite poles of cells during the first meiotic metaphase, thereby ensuring chromosome alignment and subsequent reductional segregation of chromosomes. **b**, Processes and activation-promotion are marked by continuous black arrows and red dashed arrows, respectively. DSBs are introduced into the genome by the SPO11 enzyme (left). The 5' ends of

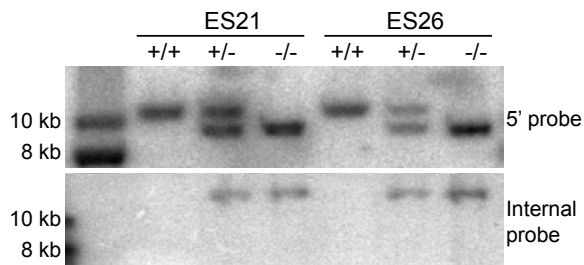
DSBs are resected and 3' single-stranded overhangs are created following removal of SPO11 from the ends of DSBs. These single-stranded DSB ends are used for homology search through strand invasion. Strand invasion into homologous sequences rather than into sister sequences is favoured during meiosis (indicated by thicker arrow in the figure). Non-homologous end joining (NHEJ) is also not favoured during meiotic DSB repair. Strand invasion events into homologues, particularly stable strand invasion events that become committed to turn into COs, promote SC initiation and formation between homologues. In turn, the SC or some of the SC components promote repair of DSBs. Of the 200-400 DSBs that are introduced into the mouse genome, only fewer than 30 are repaired as COs. Most of the remaining DSBs are believed to be repaired from homologues as non-crossover, a manifestation of which is gene conversion. The checkpoint control of CO-related prophase processes is poorly understood. Nevertheless, it is believed that unrepaired DSBs and either unsynapsed autosomes (males) or unsynapsed chromosomes (females) activate meiotic checkpoint mechanisms that eliminate defective meiocytes.

SUPPLEMENTARY INFORMATION

a



b



c

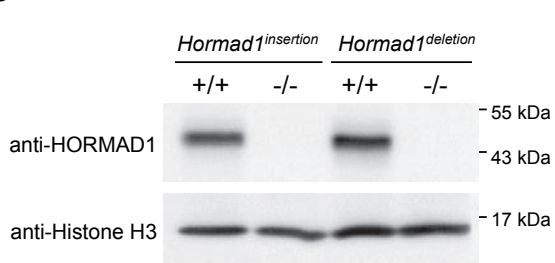


Figure S2 Generation of Hormad1-/- mice. **a**, Targeting construct, WT and modified *Hormad1* genomic locus. Black boxes represent exons (not to scale). Recombination at the homology arms (HA) of the targeting construct modifies intron 3 by introducing: 1) an additional exon (SA-IRES-LacZ-neo) that contains a strong splice acceptor site (SA) and poly-adenylation site (left grey box), 2) a transcriptional unit that contains the strong housekeeping phosphoglycerine kinase (PGK) promoter driving a Blasticidin resistance gene (BSD) as a selection marker. This modification of intron 3 disrupts the *Hormad1* ORF after the 60th codon (*Hormad1^{insertion}*). Recombination catalysed by FLPe at FRT sites removes the SA-IRES-LacZ-neo exon and the PGK-BSD gene, and restores the *Hormad1* ORF (*Hormad1^{restored}*). *Hormad1^{restored}* is a functional allele that can be disrupted by Cre-mediated recombination between loxP sites (*Hormad1^{deletion}*). Excision of exon 4 causes a frameshift after the 60th codon. The positions of

PCR-genotyping primers are indicated. Red bars mark the 5' and internal Southern blot probes; the predicted length of restriction fragments is indicated. **b**, Southern blot of DNA from WT (+/+), *Hormad1^{+/+insertion}* (+/-), *Hormad1^{insertion/insertion}* (-/-) mice derived from two independent targeted embryonic stem cell clones (ES21 and ES26). DNA was digested with Bsu36I (upper panel) or with BclI (lower panel). Both lines have a single integration of the targeting cassette in the *Hormad1* locus. **c**, Western blot analysis of extracts prepared from testes of *Hormad1^{insertion/insertion}* (-/-) mice, *Hormad1^{deletion/deletion}* (-/-) mice and their WT (+/+) litter mate controls (ES26 line). An antibody raised against the C-terminus of HORMAD1 does not detect full length HORMAD1 in *Hormad1^{insertion/insertion}* (-/-) and *Hormad1^{deletion/deletion}* (-/-) testes. The lower panel shows anti-Histone H3 western blot, which is used as a loading control. Full scan images from **b** and **c** are shown in Supplementary Information, Fig. S10.

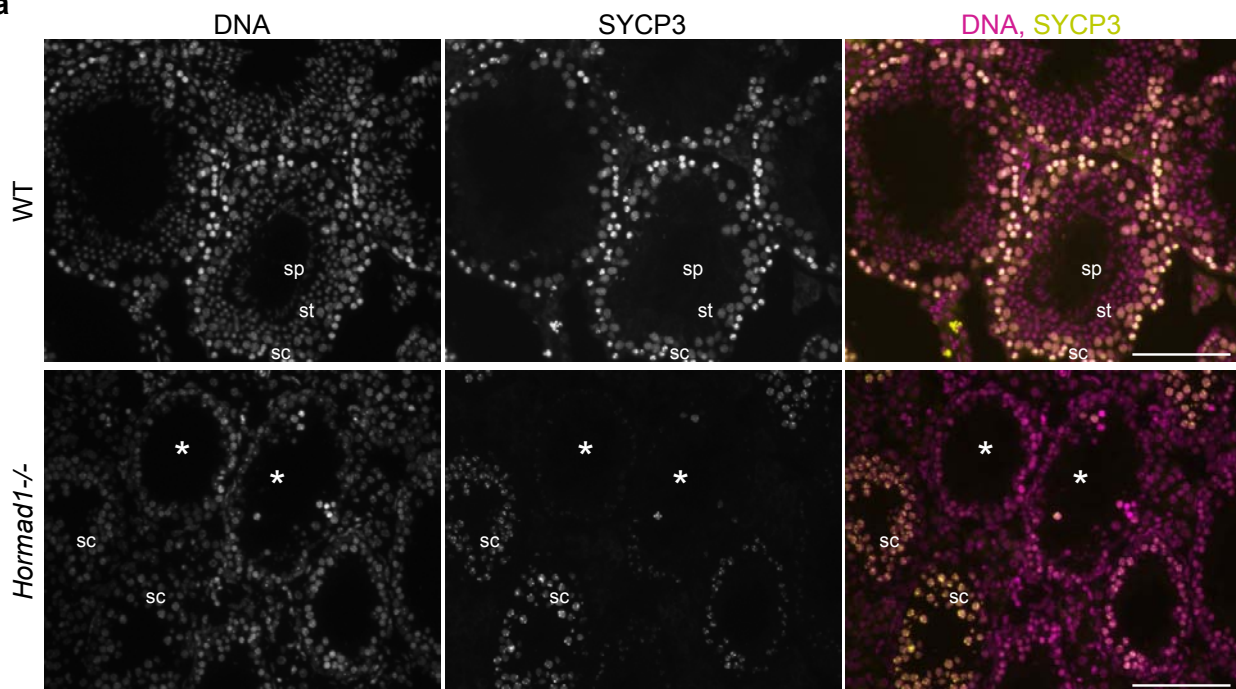
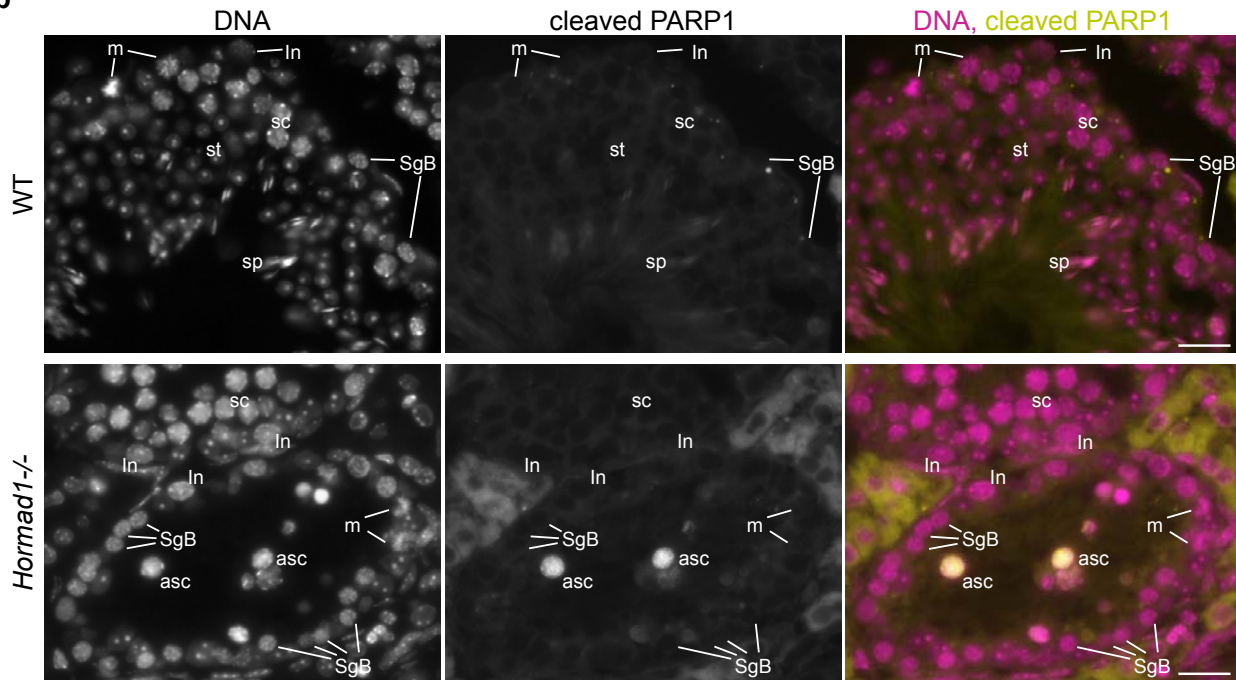
a**b**

Figure S3 Lack of HORMAD1 causes spermatogenic block at the time of mid-pachytene. **a**, Cryo-sections of testes from 11-weeks-old WT and *Hormad1*^{-/-} mice. DNA was detected by DAPI, and SYCP3 (chromosome axis) was detected by IF. Strong nuclear SYCP3 staining is characteristic of spermatocytes (sc). SYCP3-negative post-meiotic cell types: spermatids (st) and sperm (sp) are present in WT testes. No post-meiotic cells are observed in *Hormad1*^{-/-} testes. Spermatocyte-free tubules are also observed in *Hormad1*^{-/-} testes (*). **b**, To determine at what stage *Hormad1*^{-/-} cells are eliminated, DNA was detected by DAPI, and nuclear cleaved PARP1 (apoptosis marker) was detected by IF on cryo-sections of testes from

11-weeks-old mice. No apoptotic cells are detected in WT testis at late tubule stage IV as identified by the concomitant presence of intermediate spermatogonia (In), mitotic intermediate spermatogonia (m) and spermatogonia B (SgB). In *Hormad1*^{-/-} testis, spermatocytes (sc) can be found in tubule stage III-IV as identified by intermediate spermatogonia (In) (upper tubule). Most spermatocytes are eliminated and apoptotic spermatocytes (asc) are found at the end of epithelial cycle stage IV-early stage V as identified by the presence of intermediate spermatogonia (In), mitotic intermediate spermatogonia (m) and large numbers of spermatogonia B (SgB). Bars, 100 µm in **a** and 20 µm in **b**.

SUPPLEMENTARY INFORMATION

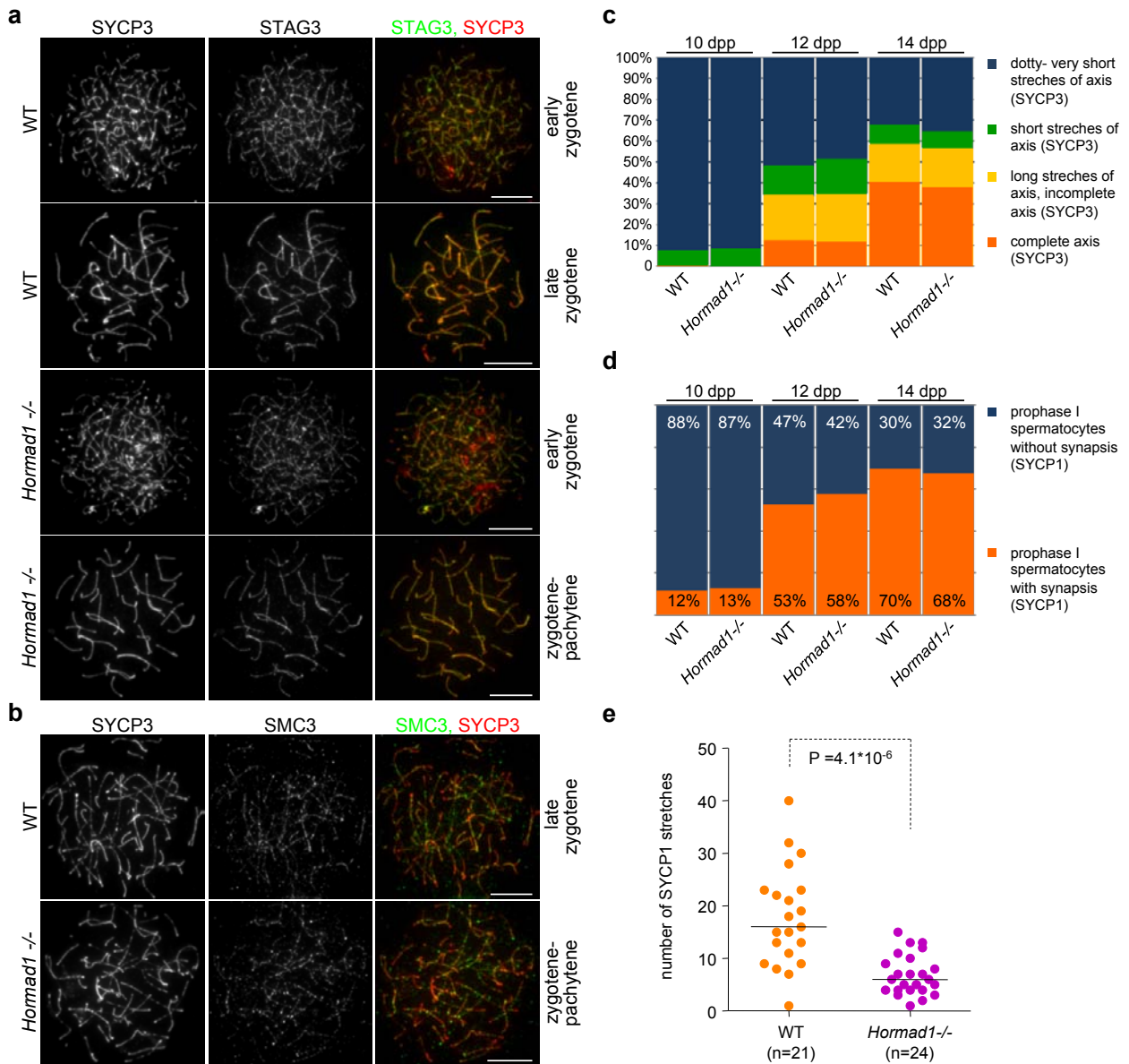


Figure S4 Cohesion core-chromosome axis development and the timing of SC formation are similar in WT and *Hormad1^{-/-}* spermatocytes. SYCP3 (chromosome axis) and either a meiosis-specific cohesin, STAG3 (**a**), or the presumed constitutive cohesion component SMC3 (**b**) were detected on nuclear spreads of spermatocytes of WT and *Hormad1^{-/-}* 29-days-old mice. No obvious difference was observed in the length of chromosome axes or in the localisation pattern of the examined cohesins in mutant and WT spermatocytes. Bars, 10 µm. **c**, Axis development was assessed through detection of SYCP3 on nuclear spreads of spermatocytes from litter mate pairs of WT and *Hormad1^{-/-}* mice at the indicated ages (days postpartum-dpp). Fractions of spermatocytes belonging to four different axis-development category are shown: dotty- very short stretches of axes, leptotene stage (blue); short stretches of axes, early-zygotene (green); relatively long stretches of axes that are not complete yet, mid-zygotene (yellow); fully formed axes, late-zygotene and pachytene stages (orange). Note that 11% of 14 dpp WT spermatocytes progressed beyond the mid-pachytene stage, as judged by the

morphology of sex chromosome axes: the X and Y chromosomes are synapsed only at their very end. These late-pachytene cells are not included into the graph, because in the *Hormad1^{-/-}* mutant the corresponding stage does not exist due to mid-pachytene apoptosis of spermatocytes (Supplementary Information, Fig. S3). **d**, SC formation was assessed in spread spermatocytes from (**c**) through detection of SYCP1 (transverse filament component) by IF. Two groups of spermatocytes were distinguished: cells with no SC formation i.e., no clear SYCP1 stretches (blue); cells with variable levels of SC formation (orange) ranging from short stretches of SCs to complete autosomal SCs (the latter is observed only in WT). Late-pachytene WT cells are not included into the figure as in (**c**). **e**, Numbers of SYCP1 stretches were counted in immunostained (anti-SYCP1 and anti-SYCP3) nuclear spreads of early-zygotene stage spermatocytes from 16-days-old WT and *Hormad1^{-/-}* mice. The median number of SYCP1 stretches is 2.3 fold lower in the mutant cells than in WT (highly significant by Mann–Whitney test), indicating that the efficiency of stable SC initiation is reduced in *Hormad1^{-/-}* spermatocytes.

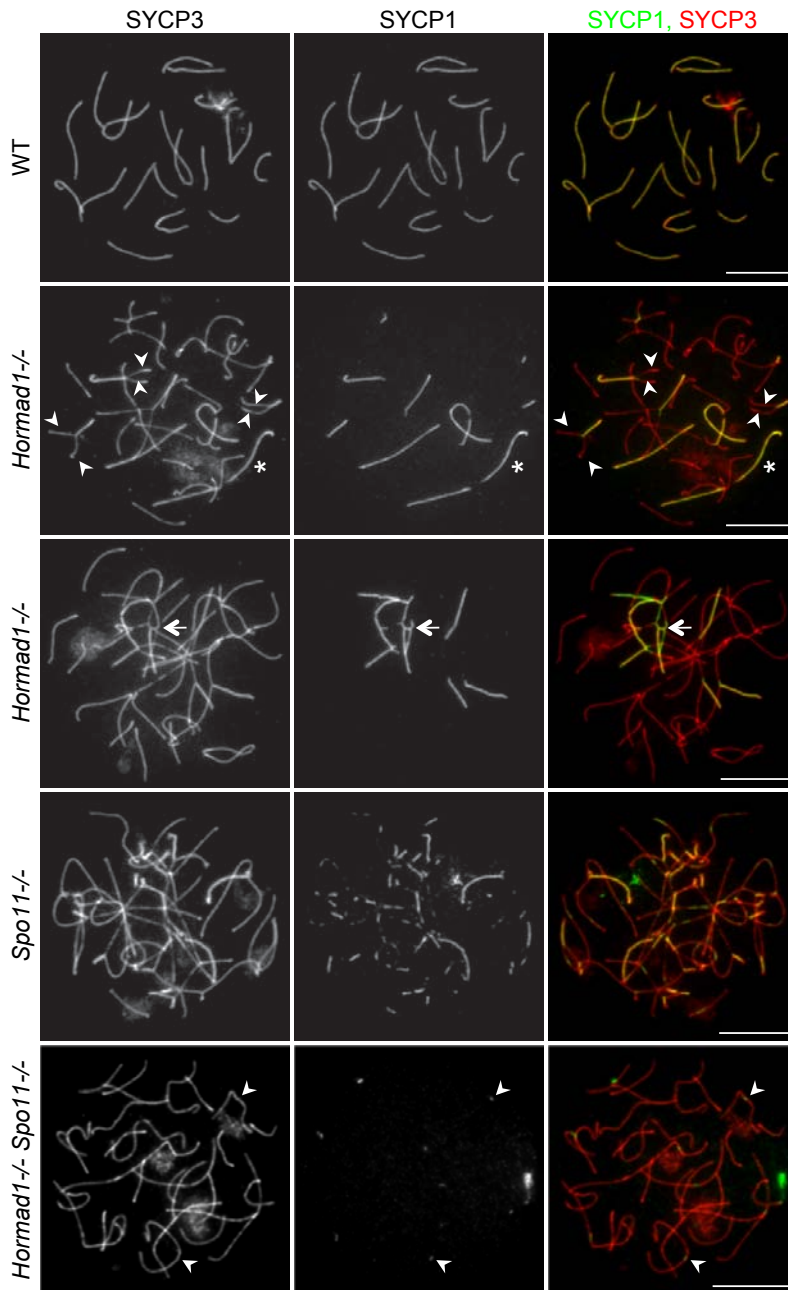


Figure S5 HORMAD1 is required for efficient SC formation in oocytes. SYCP3 (chromosome axis) and SYCP1 (SC transverse filament) are detected by IF on nuclear spreads of WT pachytene and mutant zygotene-pachytene oocytes, which were collected from ovaries at 17.5 days post coitum (dpc), when most oocytes in WT ovaries are in pachytene stage. Although a few chromosomes can synapse over their entire length (asterisk) in *Hormad1*^{-/-} cells, SC formation is never completed on all autosomes in *Hormad1*^{-/-} oocytes (n=551). Most chromosomes do not synapse or synapse only partially. Unsynapsed axes of most partially synapsed chromosomes (paired

arrowheads) are of similar lengths, indicating that most SCs form between homologues in *Hormad1*^{-/-} cells. In rare cases (1.56%, n=257), we observe SC configurations that indicate that short stretches of non-homologue SC formations (arrow) can occur in *Hormad1*^{-/-} oocytes. Non-homologous SCs frequently form in *Spo11*^{-/-} and their numbers are dramatically reduced in *Hormad1*^{-/-} *Spo11*^{-/-} spermatocytes. Note that SYCP1 stretches in the double mutant tend to be short and they do not necessarily form between two chromosomes axes (arrowheads), indicating that they do not necessarily represent functional SCs. Bars, 10 μ m.

SUPPLEMENTARY INFORMATION

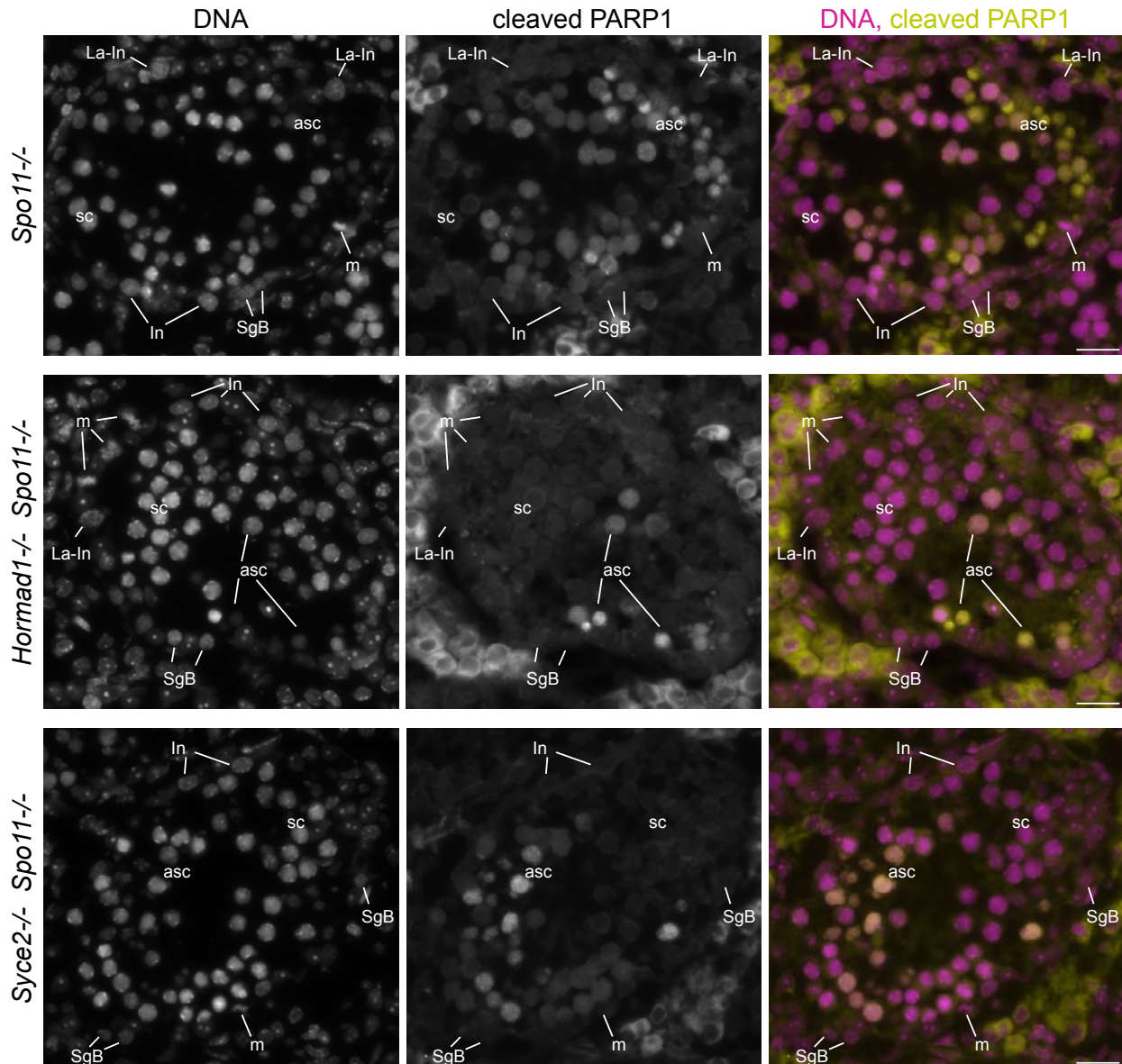


Figure S6 *Hormad1-/- Spo11-/-* spermatocytes are eliminated at stage IV, similar to *Spo11-/-* and *Syce2-/- Spo11-/-* spermatocytes. Apoptosis was examined on cryosections of testes of 11-weeks-old mice of indicated genotypes. DNA was detected by DAPI. Nuclear cleaved PARP1 (apoptosis marker) was detected by IF. *Spo11-/-*, *Hormad1-/- Spo11-/-* and *Syce2-/- Spo11-/-* spermatocytes undergo apoptosis in stage IV tubules as identified

by the concomitant presence of intermediate spermatogonia (In), late-prometaphase intermediate spermatogonia (La-In), mitotic intermediate spermatogonia (m) and spermatogonia B (SgB). Both non-apoptotic (sc) and apoptotic (asc) spermatocytes are present in the stage IV tubules shown. Spermatocytes are absent from stage V tubules of all three genotypes (data not shown). Bars, 20 μ m.

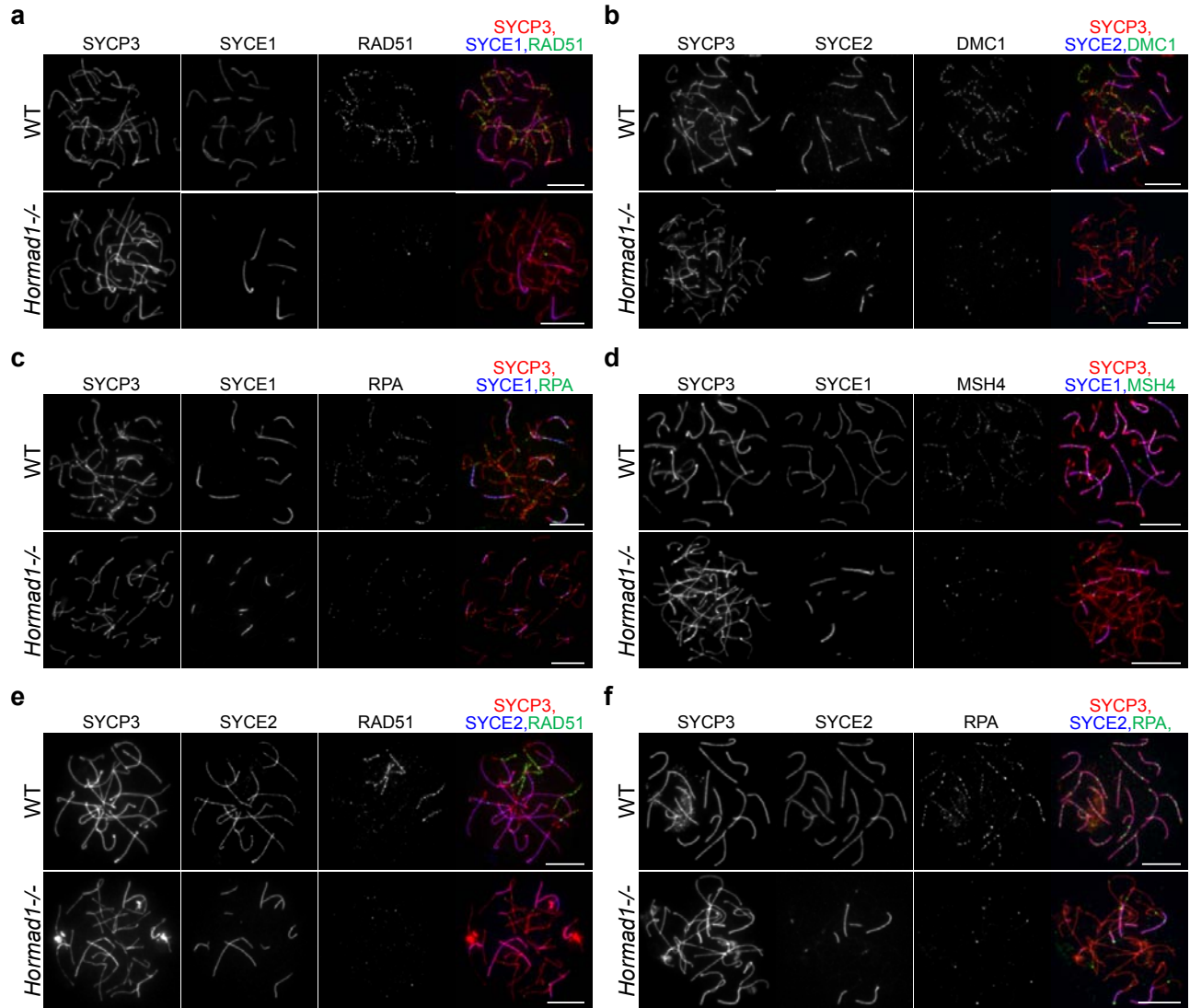


Figure S7 Numbers of early and intermediate recombination protein foci are reduced in the absence of HORMAD1 in spermatocytes and oocytes. **a-d**, Nuclear spreads of zygote WT and zygote-pachytene *Hormad1*^{-/-} spermatocytes from 15-days-old mice (**a-c**), or from adult (10-week-old) mice (**d**). Nuclear spreads were immunostained for SYCP3 (chromosome axis), SYCE1 (SC central element) and RAD51 (**a**), SYCP3, SYCE2 (SC central element) and DMC1 (**b**), SYCP3, SYCE1 and RPA (**c**), or SYCP3, SYCE1 and MSH4 (**d**). MSH4 is preferentially observed

in synapsed regions both in WT and *Hormad1*^{-/-} spermatocytes. **e** and **f**, Nuclear spreads of WT and *Hormad1*^{-/-} oocytes were immunostained for SYCP3 and SYCE2 in combination with either RAD51 (**e**) or RPA (**f**). In **e**, zygote WT and zygote-pachytene *Hormad1*^{-/-} oocytes from 16.5 dpc foetuses are shown. In **f**, pachytene WT and zygote-pachytene *Hormad1*^{-/-} oocytes from 17.5 dpc foetuses are shown. Foci of all the examined recombination proteins are fewer in *Hormad1*^{-/-} meiocytes relative to WT. Bars, 10 μm.

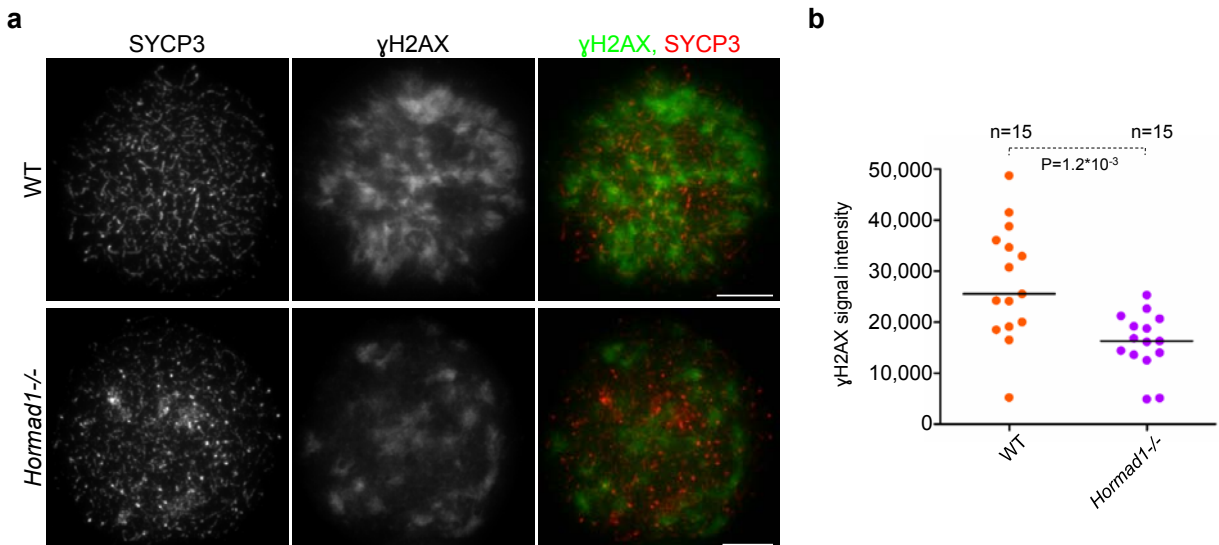


Figure S8 Chromatin bound γ H2AX levels are reduced in leptotene-early-zygotene spermatocytes in *Hormad1*^{-/-} relative to WT. **a**, SYCP3 (chromosome axis) and γ H2AX were detected by IF in nuclear spreads of leptotene-early-zygotene WT and *Hormad1*^{-/-} spermatocytes from 19-weeks-old mice. Matched exposure images of γ H2AX are shown. Note that γ H2AX levels are visibly reduced in *Hormad1*^{-/-} cells as compared to WT cell. Bars, 10 μ m. **b**, Leptotene-early-zygotene spermatocytes, as identified by the presence of short stretches of SYCP3 marked axes, have significantly

reduced total nuclear γ H2AX amounts in *Hormad1*^{-/-} mice relative to WT (Mann–Whitney test). Note that leptotene-early-zygotene cells are not homogenous populations with respect to DSB numbers (Fig. 2e-h), because DSBs are actively introduced into the genome during these stages. Variation in γ H2AX levels probably reflects this inhomogeneity. The wider range of γ H2AX levels in WT and the 1.95-fold higher maximum γ H2AX levels in WT cells may, therefore, indicate that DSB formation is less efficient in the *Hormad1*^{-/-} mutant.

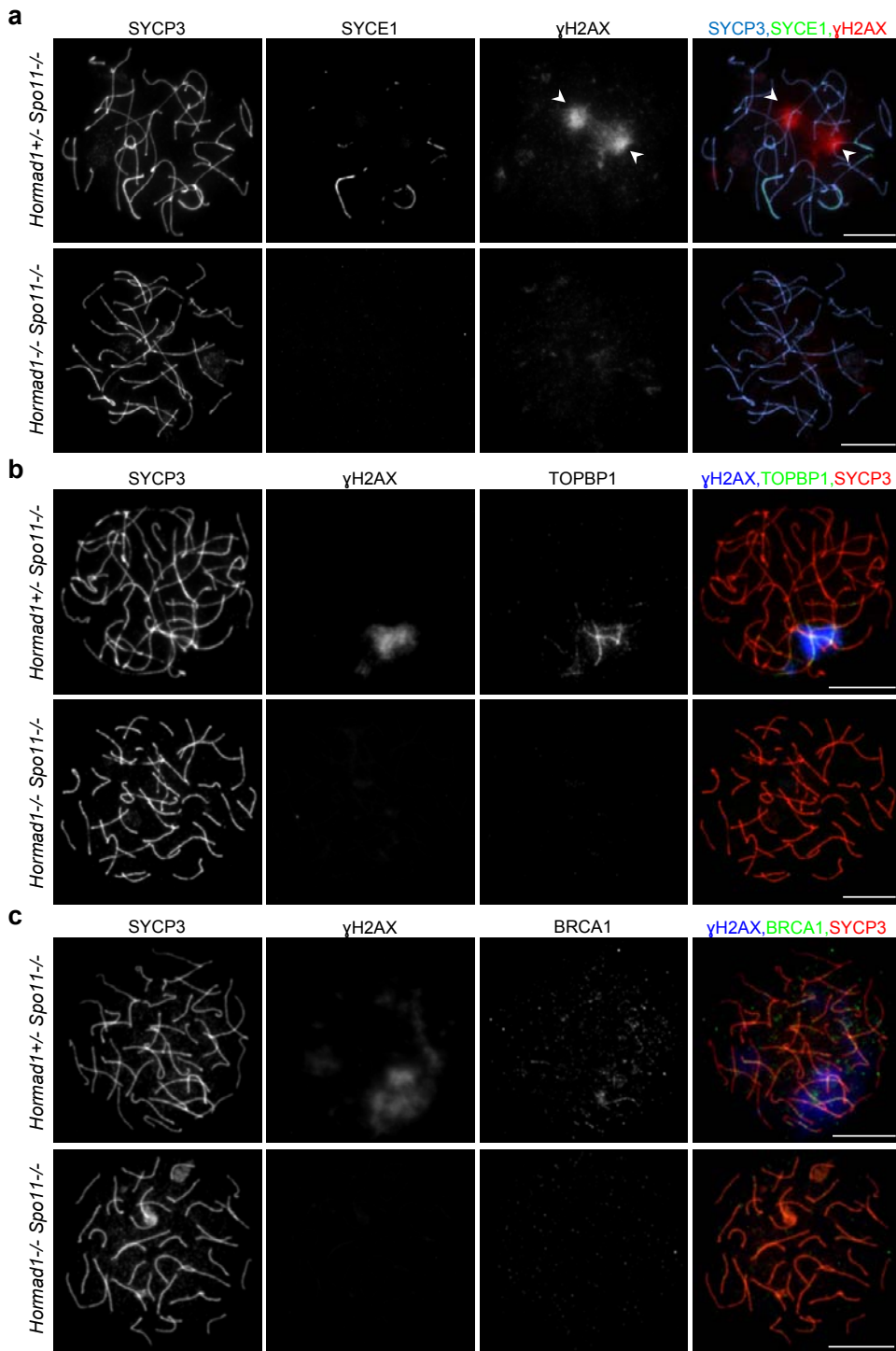


Figure S9 HORMAD1 is required for formation of γ H2AX-rich chromatin domains and for the associated accumulation of TOPBP1 and BRCA1 in *Spo11*^{-/-} oocytes. SYCP3 (chromosome axis), γ H2AX and either SYCE1 (SC central element) (a), TOPBP1 (b) or BRCA1 (c) were detected in nuclear spreads of *Hormad1*^{+/+} *Spo11*^{-/-} and *Hormad1*^{-/-} *Spo11*^{-/-} oocytes obtained from newborn litter mates. **a**, Large γ H2AX-rich chromatin domains (marked by arrowheads) are frequently observed in *Spo11*^{-/-} oocytes (65 out of 173 cells with full length chromosome axes). No large γ H2AX-rich chromatin domains could be identified in *Hormad1*^{-/-} *Spo11*^{-/-} oocytes with full length chromosome axis (n=116) at the same stage. Matched exposure images of

γ H2AX are shown. **b**, Cloud-like and axis-associated anti-TOPBP1 staining was observed in *Hormad1*^{+/+} *Spo11*^{-/-} oocytes (79 out of 251 cells with full length chromosome axes). TOPBP1 preferentially localised to γ H2AX-rich chromatin domains in these cells. Similar TOPBP1 staining was not observed in *Hormad1*^{-/-} *Spo11*^{-/-} oocytes (n=182). Matched exposure images of TOPBP1 are shown. **c**, Axis-associated BRCA1 was observed in *Hormad1*^{+/+} *Spo11*^{-/-} oocytes (83 out of 132 cells with full length chromosome axes). BRCA1 preferentially localised to γ H2AX-rich chromatin domains in these cells. Similar BRCA1 staining was not observed in *Hormad1*^{-/-} *Spo11*^{-/-} oocytes (n=89). Matched exposure images of BRCA1 are shown. Bars, 10 μ m.

SUPPLEMENTARY INFORMATION

Fig. 3a

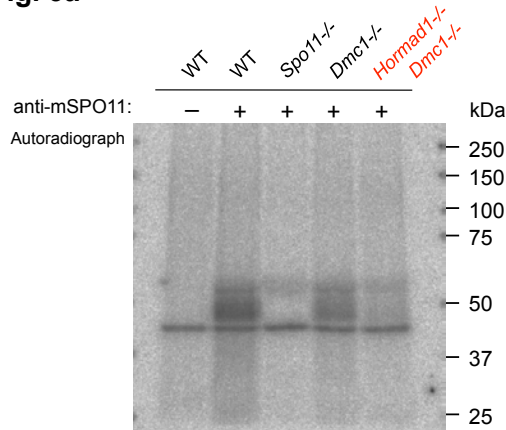


Fig. 3c

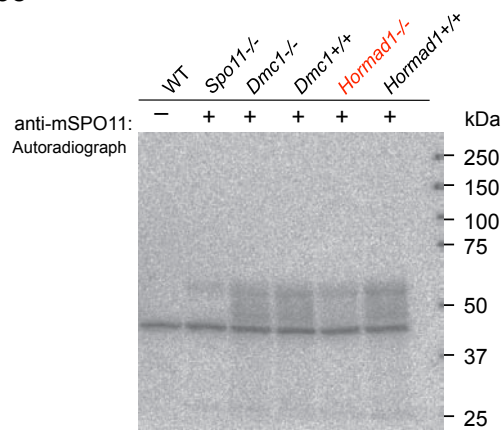


Fig. 3b

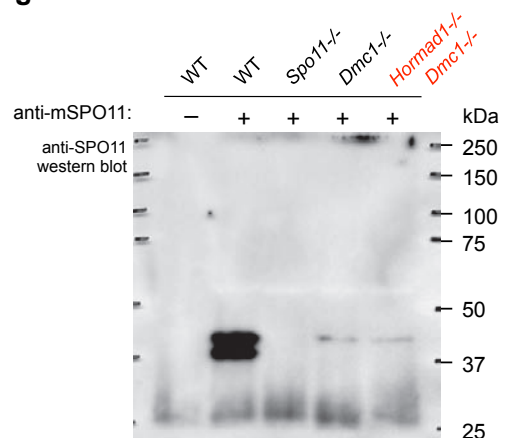
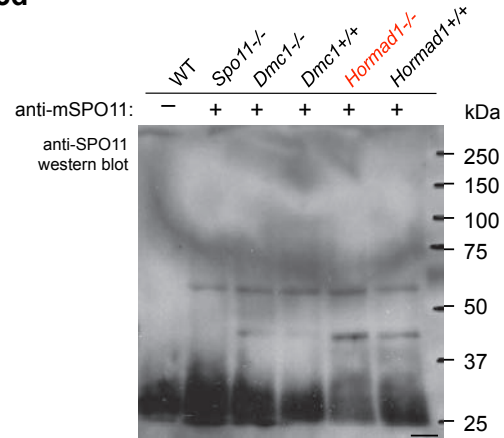
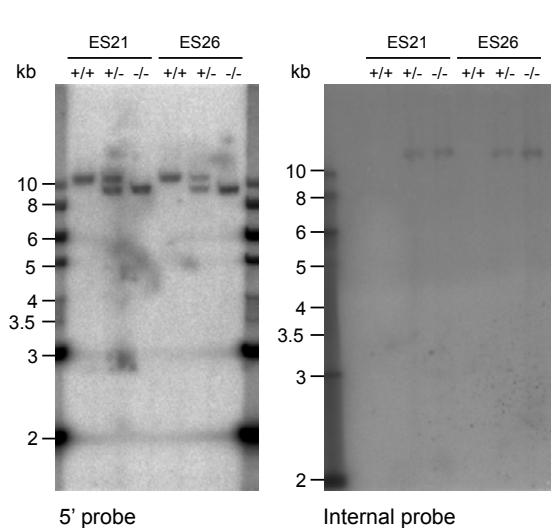


Fig. 3d



SI_Fig. S2b



SI_Fig. S2c

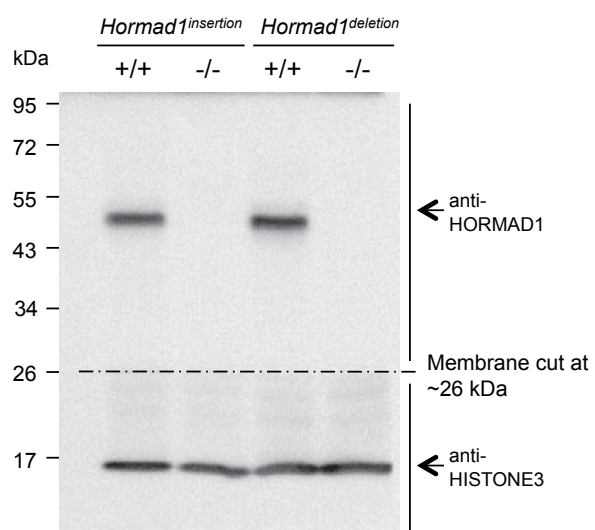


Figure S10 Full scans

Supplementary Movie Legends

Movie S1 Synchronised DIC and fluorescence movies of *in vitro*-matured *Hormad1*^{+/−} oocytes. mRNAs encoding β-tubulin-GFP and histone H2B-RFP were injected into oocytes during the germinal vesicle stage (prophase). On the left, DIC images of one optical z section are shown. On the right, an overlay of GFP (green) and RFP (red) fluorescence is shown. Each frame is a collapsed image of 8 optical sections. The movies start 5.5 h after germinal vesicle breakdown (GVBD) when oocytes are in the metaphase I stage. Images were taken every 30 min and the time after GVBD is indicated in the top right corner of the DIC movie. The first meiotic division and polar body extrusion take place 7–9 h after GVBD.

Movie S2 Synchronised DIC and fluorescence movies of *in vitro*-matured *Hormad1*^{−/−} oocytes. mRNAs encoding β-tubulin-GFP and histone H2B-RFP were injected into oocytes during the germinal vesicle stage (prophase). On the left, DIC images of one optical z section are shown. On the right, an overlay of GFP (green) and RFP (red) fluorescence is shown. Each frame is a collapsed image of 8 optical sections. The movies start 5.5 h after germinal vesicle breakdown (GVBD) when WT oocytes are in the metaphase I stage. Images were taken every 30 min and the time after GVBD is indicated in the top right corner of the DIC movie. RFP-marked chromosomes move along the abnormally long first meiotic spindle and fail to align. Only one of the 9 shown oocytes manages to extrude a polar body with great delay, 14 h after GVBD.